Journal of Computational Physics 287 (2015) 184–206

Contents lists available at ScienceDirect

Journal of Computational Physics

www.elsevier.com/locate/jcp

Asymptotic preserving scheme for the shallow water equations with source terms on unstructured meshes

A. Duran [a,b,*], F. Marche [a,b], R. Turpault [c], C. Berthon [c]

[a] I3M, Université Montpellier 2, CC 051, 34090 Montpellier, France
[b] Inria, LEMON team, 860 rue Saint-Priest, Bt 5 CC 05 017, F-34095 Montpellier, France
[c] Laboratoire de Mathématiques Jean Leray, Université de Nantes, France

ARTICLE INFO

Article history:
Received 14 November 2013
Received in revised form 3 October 2014
Accepted 3 February 2015
Available online 11 February 2015

Keywords:
Nonlinear shallow water
Asymptotic preserving
Finite volume
Friction
Well-balanced schemes
Unstructured mesh

ABSTRACT

The following work is devoted to the construction and validation of a numerical scheme for the 2D shallow water system on unstructured meshes, supplemented by topography and friction source terms. Approximate solutions of frictionless flows are obtained considering a suitable formulation of the conservation laws, involving the water free surface and some fractions of water, accounting for the topography variations. The discretization of the friction source terms relies on the use of a modified Riemann solver for the flux computation. The resulting scheme is then corrected in order to achieve an asymptotic regime preservation. A MUSCL reconstruction is also performed to increase the space order of accuracy. The overall numerical approach is shown to be consistent, well-balanced and to satisfy a domain invariant principle. These results are assessed through several benchmark tests, involving complex geometry and varying bathymetry. In the presence of dry areas, special interest is given to the wave front speed computation, highlighting the stability of the method, even when implementing the asymptotic preserving correction.

0. Introduction

Since the last decades, the necessity of finding numerical approaches providing relevant descriptions of hydrodynamic processes has been the source of many studies. Lots of numerical models are now available, relying on finite volume, finite elements, or disntinuous Galerkin methods for example. In the present work, we consider the classical Nonlinear Shallow Water (NSW in the following) equations:

$$\partial_t w + \nabla.\mathcal{H}(w) = \mathcal{B}(w,z) + \mathcal{F}(w), \tag{1}$$

where

$$w = \begin{pmatrix} h \\ q_x \\ q_y \end{pmatrix}, \quad \mathcal{H}(w) = \begin{pmatrix} q_x & q_y \\ \frac{q_x^2}{h} + \frac{1}{2}gh^2 & \frac{q_x q_y}{h} \\ \frac{q_x q_y}{h} & \frac{q_y^2}{h} + \frac{1}{2}gh^2 \end{pmatrix}, \tag{2}$$

* Corresponding author.
E-mail addresses: Arnaud.Duran@math.univ-montp2.fr (A. Duran), Fabien.Marche@math.univ-montp2.fr (F. Marche), Rodolphe.Turpault@univ-nantes.fr (R. Turpault), Christophe.Berthon@univ-nantes.fr (C. Berthon).

http://dx.doi.org/10.1016/j.jcp.2015.02.007
0021-9991/

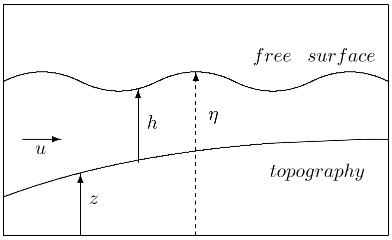

Fig. 1. Non-conservative variables for NSW equations.

and the bathymetry and friction source terms are defined by:

$$\mathcal{B}(w,z) = -\begin{pmatrix} 0 \\ ghz_x \\ ghz_y \end{pmatrix} \quad , \quad \mathcal{F}(w) = -\begin{pmatrix} 0 \\ n^2 \frac{\sqrt{q_x^2+q_y^2}}{h^\gamma} q_x \\ n^2 \frac{\sqrt{q_x^2+q_y^2}}{h^\gamma} q_y \end{pmatrix}. \tag{3}$$

Herein, ∂_t stands for the time derivative, h is the water height, z the bed elevation and $\mathbf{q} = {}^t(q_x, q_y)$ is the discharge vector. We also set $\mathbf{u} = {}^t(u, v)$ for the primitive variables, so that we have $\mathbf{q} = h\mathbf{u}$. The free surface is defined by $\eta = h + z$ (see Fig. 1). Finally, n and γ stand for two positive parameters governing the Manning friction law.

The major goals in the construction of an efficient shallow water numerical model are various. A first essential condition for a suitable discretization is the so-called "well balancing" property, namely the ability to preserve the *still water steady states*:

$$\eta = cte \quad \text{and} \quad \mathbf{u} = 0. \tag{4}$$

Generally, a direct numerical approach does not lead to a well balanced scheme. Since the pioneering works [6] and [43], the interest for formulations providing an exact preservation of steady states has grown and a lot of studies can be found (we refer to [16] for a general overview). Regarding the specific case of shallow water flows, the *hydrostatic reconstruction* proposed in [2] has been intensively used or studied in recent years [3,25,33,37,38,57,59,65]. Many other works and efficient numerical methods can also be found in the literature, see for instance [5,26,34,45,47,55,60,61,64]. We notice that all the above-mentioned schemes have in common the set of equations (1) as starting point. There are however other convenient ways to formulate these equations. For instance, the so-called *pre-balanced* NSW equations offer a privileged framework in regard to the well balancing property and the discretization of the bed elevation. This formulation is used in [53,36,48,50] and similar practical ideas can also be encountered in [20], or [51,67], where 2D well balanced schemes on Cartesian grids are proposed. Another method consists of introducing a new variable as a fraction of water: $\xi = \frac{h}{\eta}$, see [9], leading to a simple well balanced system, with an excellent behavior for low level of water surface. Extension to the 2D unstructured case is carried out in the present work, using a convex combination of 3 points one-dimensional schemes.

A second unavoidable requirement is the preservation of the water height positivity, which is closely related to the problem of flooding and drying. The description of hydrodynamic processes like run-up phenomena or flooding waves in dam-breaks requires numerical approaches that allow to accurately deal with the occurrence of dry states. The simulation of such flows in coastal areas or dry bed rivers is far from being obvious, as the treatment of wet/dry interfaces is generally coupled with complex geometry and bathymetry. We refer to [3,9,14,15,36,37,40,48,52,61,66] for instance for discussions on the robustness property and flooding and drying in the frictionless 2D case. Note however that when dealing with the issue of preserving the positivity of the water depth, one of the major problems stands in finding a reasonable time step limitation and it is interesting to see that the so-called *draining time step* introduced in [15], based on a separation of the inflow and outflow contributions, shares some similarities with the restriction proposed in [9].

When friction source terms under the general form (3) are involved, the issue of robustness becomes all the more important. Indeed, full consideration has to be given to the discretization of the additional physical resistance component, as the asymptotic behavior of $\mathcal{F}$ with respect to low values of h may possibly lead to unstable computations. This problematic is clearly underlined in [11,18,49] for instance. In a 2D unstructured framework, the semi-implicit approaches proposed in [19,26,34,58] are one of the few schemes able to cure such instabilities. In [11], a new approach is introduced, based on the use of a modified Riemann solver that directly accounts for friction effects; the resulting scheme is shown to be robust and to offer very accurate results in a variety of complex situations.

Following these lines, we introduce in the present work a robust and well-balanced two dimensional extension based on the ideas of [11], providing accurate and stable computations in the vicinity of dry cells. Additionally, this method allows us to introduce a relevant asymptotic preserving correction to the resulting scheme.

Indeed, many theoretical and numerical studies devoted to the asymptotic behavior of 1D conservation laws appeared in the last decades. A lot of numerical schemes are now designed to restore the asymptotic regime of the corresponding equations. Such numerical methods are commonly called "Asymptotic Preserving" (AP). We can mention for instance [7,8,10] and [22,21] for the M1 model for radiative transfer, or [17,28,56] for the discretization of Euler equations. Several other systems have been treated, such as the Boltzmann kinetic model [41,54], or Euler–Poisson system [31,44] for instance. The reader is also referred to [1,13,30,42,44] for additional studies. In the 2D case, the quantity of published results is definitively less abundant. On Cartesian grids, in addition of [8], we can refer to [32] for the Euler–Lorentz system. In an unstructured meshes context, the extrapolation technique developed in [39] is, to our knowledge, the only method available to date (see also [23]). Although the issue of the 1D NSW equations has been considered is some studies [10,29,46,44], no asymptotic preserving scheme has already been developed for the 2D equations in the framework of unstructured meshes.

Thus, in what follows, we propose the construction and validation of an asymptotic preserving numerical scheme for the 2D shallow water model, accounting for topography and friction source terms. To achieve this, following the lines of [12] for the telegraph equations, Euler equations with high friction, or the M1 model developed by Dubroca et al. [35], we introduce a relevant correction in order to recover a discrete version of the diffusive limit observed by the governing equations. The efficiency of asymptotic preserving schemes has been extensively pointed out in the above references and we also aim at highlighting its benefits for the NSW equations.

The remainder of this paper is organized as follows: in the first part we focus on the asymptotic analysis, detailing the derivation of the late-time diffusive regime satisfied by the NSW equations in 2D with a quadratic friction term. In the next parts, we recall the well-balanced discretization of the NSW equations proposed in [9], focusing on the 2D case with unstructured meshes, and we introduce the new friction term discretization, extending the ideas developed in [12] to the 2D case. Then, we investigate the issue of the asymptotic preserving correction, to recover the singular regime exhibited in Section 1. We lastly detail a MUSCL-like reconstruction in order to achieve a formal second order accuracy before highlighting the abilities of the new approach through several benchmark tests.

1. Asymptotic regime for NSW

We investigate in this first section the formal derivation of the equation driving the late-time asymptotic behavior of general solutions of the NSW equations with a quadratic Manning-like friction source term, as stated in (1). Following the lines of [12,10], we introduce a rescaling parameter $\varepsilon > 0$, and consider the following set of equations:

$$\epsilon\,\partial_t h^\epsilon + \partial_x q_x^\epsilon + \partial_y q_y^\epsilon = 0\,, \tag{5}$$

$$\epsilon\,\partial_t q_x^\epsilon + \partial_x\left((q_x^\epsilon)^2/h^\epsilon + \frac{1}{2}g(h^\epsilon)^2\right) + \partial_y\left(q_x^\epsilon q_y^\epsilon/h^\epsilon\right) = -gh^\epsilon\,\partial_x z - g\frac{\varrho^2(h^\epsilon)}{\epsilon^2}\|\mathbf{q}\|q_x^\epsilon\,, \tag{6}$$

$$\epsilon\,\partial_t q_y^\epsilon + \partial_x\left(q_x^\epsilon q_y^\epsilon/h^\epsilon\right) + \partial_y\left((q_y^\epsilon)^2/h^\epsilon + \frac{1}{2}g(h^\epsilon)^2\right) = -gh^\epsilon\,\partial_y z - g\frac{\varrho^2(h^\epsilon)}{\epsilon^2}\|\mathbf{q}\|q_y^\epsilon\,, \tag{7}$$

in which we rewrite the friction term, setting $g\varrho^2(h) = \frac{n^2}{h^\gamma}$.

We highlight that the stiff relaxation source term involved in (6)–(7) introduces an additional scale in the problem, defined in accordance with the specific nonlinearity of the friction source term (quadratic function of $\mathbf{q}$). This system enters the framework of the generalized analysis proposed in [10], that encompasses models with strong nonlinearities in the relaxation and in the following, we focus on its asymptotic behavior in the singular regime $\varepsilon \to 0$.

In the spirit of Chapman–Enskog expansions [27], let us perform formal expansions of each component of the conservative variables vector:

$$w^\epsilon = w^0 + \epsilon\, w^1 + O(\epsilon^2)\,. \tag{8}$$

Considering that Eqs. (6) and (7) have to be relevant whenever ϵ tends to zero, we necessarily have $q_x^0 = q_y^0 = 0$, and the following relations are satisfied by the discharge components:

$$gh^0\partial_x(h^0+z) = -g\varrho^2(h^\epsilon)\|\mathbf{q}\|q_x^1\,,$$
$$gh^0\partial_y(h^0+z) = -g\varrho^2(h^\epsilon)\|\mathbf{q}\|q_y^1\,.$$

After some algebraic manipulations, we obtain:

$$q_x^1 = -\frac{\sqrt{h^0}}{\varrho(h^\epsilon)}\frac{\partial_x(h^0+z)}{\sqrt{\|\nabla(h^0+z)\|}},$$
$$q_y^1 = -\frac{\sqrt{h^0}}{\varrho(h^\epsilon)}\frac{\partial_y(h^0+z)}{\sqrt{\|\nabla(h^0+z)\|}},$$

so that the Chapman–Enskog expansion in (5) yields the following *non-linear* diffusive regime:

$$\partial_t h - \nabla\cdot\left(\frac{\sqrt{h}}{\varrho(h)\sqrt{\|\nabla\eta\|}}\nabla\eta\right) = 0\,, \tag{9}$$

which is nothing but the generalized 2D version, accounting for varying bottoms, of the equations obtained in [10]. In the following, we introduce a new discretization of (1) on unstructured meshes, that accounts for the quadratic friction term.

- K_i : set of subscripts j for which C_j is adjacent to C_i.
- $|C_i|$: area of C_i.
- Γ_{ij} : boundary interface defined by C_i and C_j.
- ℓ_{ij} : length of Γ_{ij}.
- $\vec{n}_{ij}$: unit normal to Γ_{ij} pointing to C_j.

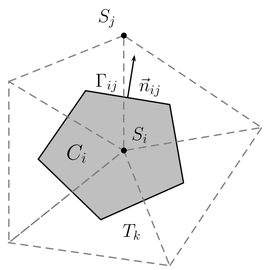

Fig. 2. Vertex centered formalism: notations and geometry.

Eq. (9) will be considered in Section 4, in which a suitable correction of the source term discretization is proposed, allowing us to recover this expected asymptotic regime.

2. Frictionless scheme

In this section, for the sake of completeness, we expose the broad lines of the well-balanced *hydrostatic upwind scheme* developed in [9] that will constitute the basis of the numerical model. Let us introduce the new variable $W = (\eta, \eta u, \eta v)$ and the following formulation of the NSW equations:

$$\partial_t w + \nabla . \left(\xi \mathcal{H}(W) - \begin{pmatrix} 0 & 0 \\ \dfrac{ghz}{2} & 0 \\ 0 & \dfrac{ghz}{2} \end{pmatrix} \right) = 0 \,, \tag{10}$$

where $\xi = \frac{h}{\eta}$ and $\mathcal{H}$, w are given by the set of Eqs. (1), (2). We consider the dual mesh issuing from a triangulation $\mathcal{T}$ of the computational domain. The nodes of $\mathcal{T}$ will be denoted $(S_i)_i$, and the elements $(T_i)_i$. On each vertex cell C_i, we denote $w_i^n = (h_i^n, (q_x)_i^n, (q_y)_i^n)$ a constant approximation of the exact solution at time t^n; other useful notations are also introduced in Fig. 2. As also detailed in [9], the scheme's conception relies on the use of a convex combination:

$$w_i^{n+1} = \sum_{j \in K_i} \frac{|T_{ij}|}{C_i} \tilde{w}_{ij}^{n+1} \,, \tag{11}$$

where each contribution can be interpreted as coming from a 1D-like scheme (see Figs. 2 and 3):

$$\tilde{w}_{ij}^{n+1} = w_i^n - \frac{\Delta t}{\Delta_{ij}} \left[\phi(w_i^n, w_j^n, \vec{n}_{ij}) - \phi(w_i^n, w_i^n, \vec{n}_{ij}) \right] + \frac{\Delta t}{\Delta_{ij}} B_{ij} \,, \tag{12}$$

with the following notations:

- $\Delta_{ij} = \dfrac{|T_{ij}|}{l_{ij}}$,
- $\phi(w_i^n, w_j^n, \vec{n}_{ij}) = \mathcal{X}_{ij} H(W_i^n, W_j^n, \vec{n}_{ij})$,
- $H = H(U, V, \vec{n})$ denotes an approximation of the normal component of the exact flux function $\mathcal{H} \cdot \vec{n}$,
- $\mathcal{X}_{ij}$ and $\mathcal{N}_{ij}$ are given by the following transport relations:

$$\mathcal{X}_{ij} = \begin{cases} \xi_i^n & \text{if} \quad H^h(W_i^n, W_j^n, \vec{n}_{ij}) \geq 0 \,, \\ \xi_j^n & \text{otherwise,} \end{cases} \tag{13}$$

$$\mathcal{N}_{ij} = \begin{cases} \eta_i^n & \text{if} \quad H^h(W_i^n, W_j^n, \vec{n}_{ij}) \geq 0 \,, \\ \eta_j^n & \text{otherwise.} \end{cases} \tag{14}$$

- B_{ij} is the discretization of the bed slope:

$$B_{ij} = \frac{g}{2} \begin{pmatrix} 0 \\ \mathcal{N}_{ii} \mathcal{N}_{ij} (\mathcal{X}_{ij} - \mathcal{X}_{ii}) \vec{n}_{ij} \end{pmatrix} . \tag{15}$$

Remark 2.1. As highlighted in [9], the NSW system (1) only involves variations of the bed slope, and is free from the definition of the bottom. Thus, we suppose that the minimum value of z is positive within the computational domain, giving sense to the definition of ξ.

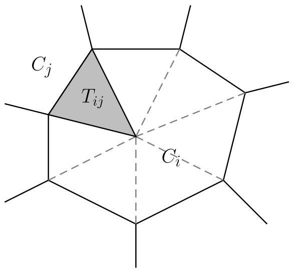

Fig. 3. Dual cell C_i and associated subgrid.

Remark 2.2. The evaluation of the numerical flux function H is classically based on the use of an approximate Riemann solver in the normal reference associated with the interface Γ. Such function would be supposed to be consistent with the exact flux $\mathcal{H}$:

$$H(W, W, \vec{n}) = \mathcal{H}(W) \cdot \vec{n} \quad \forall W \in \Omega, \tag{16}$$

and satisfy the conservativity property:

$$H(U, V, \vec{n}) = -H(V, U, -\vec{n}) \quad \forall U, V \in \Omega. \tag{17}$$

In the above-mentioned properties, $\Omega := \{(h, hu, hv),\ h \geq 0\}$ stands for the set of admissible states. In the following, we will also denote $a_{ij}^{\pm}$ the maximum and minimum wave speeds involved in the Riemann solver during the evaluation of the flux at the interface Γ_{ij}.

Remark 2.3. The values in (12) are evolved in time with the classical Euler scheme. Therefore, more accurate time marching methods can be used. In this work, only fully explicit Euler or Runge–Kutta methods will be considered. Thus, whenever possible, the subscript n referring to time t^n will be ignored.

Using formula (11), we obtain, after straightforward computations involving discrete Green formula:

$$w_i^{n+1} = w_i^n - \frac{\Delta t}{|C_i|} \sum_{j \in K_i} l_{ij} \phi(w_i, w_j, \vec{n}_{ij}) + \frac{\Delta t}{|C_i|} \sum_{j \in K_i} l_{ij} B_{ij}. \tag{18}$$

We can already emphasize that robustness and well-balancing properties are straightly inherited from the 1D scheme. More precisely:

Theorem 2.4. *We consider a numerical flux function H consistent with the exact flux in the sense of (16), verifying the conservativity property (17). Assume that $(w_i^n)_{i\in\mathbb{Z}}$ belongs to Ω. We consider the updated states $(w_i^{n+1})_{i\in\mathbb{Z}}$ obtained with the scheme (18).*

1 *Robustness: under the following CFL condition:*

$$\Delta t \max_{i\in\mathbb{Z},\ j\in K_i} \frac{l_{ij}}{|T_{ij}|} |a_{ij}^{\pm}| \leq \frac{1}{2}, \tag{19}$$

supplemented by the following CFL restriction:

$$\Delta t \max_{i\in\mathbb{Z},\ j\in K_i} \left[\frac{l_{ij}}{|T_{ij}|} \Big(\max\left(0, H^h(W_i, W_j, \vec{n}_{ij})\right) - \min\left(0, \mathcal{H}^h(W_i).\vec{n}_{ij}\right) \Big) \right] < \eta_i, \tag{20}$$

we have $h_i^{n+1} \geq 0$, for all $i \in \mathbb{Z}$.

2 *Well balancing: assume $u_i^n = u_j^n = 0$ and $\eta_i^n = \eta_j^n = \eta$ for all $j \in K_i$. Then $u_i^{n+1} = 0$ and $\eta_i^{n+1} = \eta$.*

Proof. We consider the formulation (11), (12), together with the robustness and well balancing properties of the 1D scheme. See [9] for details. A more complete analysis will be conducted later, with the inclusion of friction. □

Remark 2.5. Note that the time step limitation (20) can be interpreted as resulting from an analysis of the outflow and inflow parts of the numerical fluxes appearing in the 1D scheme. Such a separation between outflow and inflow contributions is also performed in [15], allowing to obtain the preservation of the water height positivity under the so-called "*draining time*" CFL.

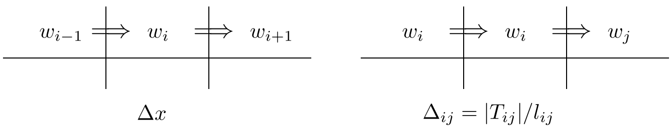

Fig. 4. Left and right Riemann states for the 1D and 2D schemes.

3. Discretization of the friction source term

Let us now face the issue of the discretization of the friction term. For the sake of clarity, we consider the Manning formulation appearing in (3), but other formulations can be of course addressed in the same way. We consider the set of equations (10) supplemented with the friction source term, recast under the following form:

$$\mathcal{F}(w) = \sigma(R(w) - w), \tag{21}$$

with:

$$\sigma = \sigma(h) = \frac{n^2}{h^\gamma} \quad , \quad R(w) = {}^t(h, q_x - \|\mathbf{q}\| q_x, q_y - \|\mathbf{q}\| q_y). \tag{22}$$

Extending the ideas introduced in [12], we suggest to extend the approach to a two-dimensional framework (Fig. 4), modifying each component of the convex combination (12) as follows:

$$\tilde{w}_{ij}^{n+1} = w_i^n - \frac{\Delta t}{\Delta_{ij}}\Big[\alpha_{ij}\phi(w_i, w_j, \vec{n}_{ij}) - \alpha_{ij}^c \phi(w_i, w_i, \vec{n}_{ij})\Big] + \frac{\Delta t}{\Delta_{ij}} \Delta S_{ij} + \frac{\Delta t}{\Delta_{ij}} B_{ij}, \tag{23}$$

where

$$\Delta S_{ij} = (1 - \alpha_{ij}^c) S_{ii}^+ + (1 - \alpha_{ij}) S_{ij}^-, \tag{24}$$

with

$$S_{ii}^+ = \max(0, a_{ii}^-)\,(w_i - R(w_i)) + \max(0, a_{ii}^+)\,(R(w_i) - w_i) + \phi(w_i, w_i, \vec{n}_{ij}),$$
$$S_{ij}^- = \min(0, a_{ij}^-)\,(w_i - R(w_i)) + \min(0, a_{ij}^+)\,\big(R(w_i) - w_j\big) - \phi(w_i, w_i, \vec{n}_{ij}).$$

Remark 3.1. In a 1D context, the scheme (23) results from the use of a modified approximate Riemann solver with an additional stationary wave, in which the intermediate states are expressed as follows:

$$\tilde{w}_{\mathcal{R}}(\frac{x}{t}, w_L, w_R) = \begin{cases} w_L & \text{if } \frac{x}{t} \le a^-, \\ \alpha w^* + (1-\alpha) R(0^-, w_L) & \text{if } \min(0, a^-) \le \frac{x}{t} \le \min(0, a^+), \\ \alpha w^* + (1-\alpha) R(0^+, w_R) & \text{if } \max(0, a^-) \le \frac{x}{t} \le \max(0, a^+), \\ w_R & \text{if } \frac{x}{t} \ge a^+. \end{cases} \tag{25}$$

Herein, w^* stands for the intermediate state involved in the solver under consideration, and $a^\pm$ are the upper and lower extremities of the dependency cone related to the approximate Riemann solver, with $R(0^\pm, w) := \lim\limits_{x \to 0^\pm} R(x, w)$, allowing the occurrence of discontinuities. The reader is referred to [12] for a detailed study of the one dimensional scheme (23).

We investigate now the issue of a relevant choice for the free parameters $\alpha_{ij}^c, \alpha_{ij}$. Following [12,11], the requirements under consideration are mainly controlled by consistency relations. To simplify the subsequent developments, we choose now to consider the following Rusanov approximate flux function:

$$H(W_i, W_j, \vec{n}_{ij}) = \frac{1}{2}\big(\mathcal{H}(W_i)\cdot\vec{n}_{ij} + \mathcal{H}(W_j)\cdot\vec{n}_{ij}\big) - \frac{a_{ij}}{2}\left(W_j - W_i\right), \tag{26}$$

where

$$a_{ij} = \max(|u_i \pm c_i|, |u_j \pm c_j|). \tag{27}$$

In other words, we define the maximum and minimum characteristic speeds in the HLL Riemann solver as: $a_{ij}^\pm = \pm a_{ij}$.

This particular choice allows convenient simplifications for the friction terms, since we have now:

$$S_{ii}^+ = a_{ii}\big(R(w_i) - w_i\big) + \phi(w_i, w_i, \vec{n}_{ij}) \quad , \quad S_{ij}^- = -a_{ij}\big(w_i - R(w_i)\big) - \phi(w_i, w_i, \vec{n}_{ij}), \tag{28}$$

according to (24) and the definition of the wave speeds (27). Then, getting back to formulation (11), (23), we obtain, after straightforward computations:

$$
\begin{aligned}
w_i^{n+1} = w_i^n &- \frac{\Delta t}{|C_i|} \sum_{j\in K_i} l_{ij}\big[\alpha_{ij}\phi(w_i, w_j, \vec{n}_{ij}) - \alpha_{ij}\phi(w_i, w_i, \vec{n}_{ij})\big] \\
&+ \frac{\Delta t}{|C_i|} \sum_{j\in K_i} l_{ij}\Delta F_{ij} + \frac{\Delta t}{|C_i|} \sum_{j\in K_i} l_{ij} B_{ij} ,
\end{aligned} \tag{29}
$$

with

$$
\begin{aligned}
&\Delta F_{ij} = (1-\alpha_{ij}^c)F_{ii}^+ + (1-\alpha_{ij})F_{ij}^- , \\
&F_{ii}^+ = a_{ii}\big(R(w_i) - w_i\big) \quad , \quad F_{ij}^- = -a_{ij}\big(w_i - R(w_i)\big) .
\end{aligned} \tag{30}
$$

As stated in the following lines, a possible choice for the friction parameters is thus given by:

$$
\begin{aligned}
&\alpha_{ij}^c = \frac{2\nu_i a_{ii}}{2\nu_i a_{ii} + \sigma_{ii}\frac{|C_i|}{l_{ij}}} , \ \sigma_{ii} = \sigma(w_i) , \\
&\alpha_{ij} = \frac{2\nu_i a_{ij}}{2\nu_i a_{ij} + \sigma_{ij}\frac{|C_i|}{l_{ij}}} , \ \sigma_{ij} = \frac{n^2}{(h_i^\gamma + h_j^\gamma)/2} ,
\end{aligned} \tag{31}
$$

where ν_i stands for the number of cells surrounding C_i. In particular, we have the following consistency result:

Proposition 1. *The discretization of the friction source term given by (29), (31) is consistent with the additional source term $\sigma(R(w) - w)$ (21) of the continuous equations.*

Proof. We first notice that:

$$
\begin{aligned}
&\frac{l_{ij}}{|C_i|}(1-\alpha_{ij}^c) = \frac{\sigma_{ii}}{2\nu_i a_{ii} + \sigma_{ii}\frac{|C_i|}{l_{ij}}} , \\
&\frac{l_{ij}}{|C_i|}(1-\alpha_{ij}) = \frac{\sigma_{ij}}{2\nu_i a_{ij} + \sigma_{ij}\frac{|C_i|}{l_{ij}}} ,
\end{aligned}
$$

and study the behavior of the source term $\mathcal{F}_i := \sum_{j\in\nu_i} \frac{l_{ij}}{|C_i|}\Delta F_{ij}$ as $r_i = diam(C_i)$ tends to zero. We can easily check that we have:

$$
\lim_{r_i\to 0} \frac{l_{ij}}{|C_i|}(1-\alpha_{ij}^c)F_{ii}^+ = \lim_{r_i\to 0} \frac{l_{ij}}{|C_i|}(1-\alpha_{ij})F_{ij}^- = \frac{\sigma(w_i)}{2\nu_i}(R(w_i) - w_i) . \tag{32}
$$

Consequently:

$$
\begin{aligned}
\lim_{r_i\to 0} \mathcal{F}_i &= \sum_{j\in K_i} \Big[\frac{\sigma(w_i)}{2\nu_i}(R(w_i) - w_i) + \frac{\sigma(w_i)}{2\nu_i}(R(w_i) - w_i)\Big] \\
&= \sigma(w_i)(R(w_i) - w_i) . \qquad \square
\end{aligned} \tag{33}
$$

We now show that the use of such weighted fluxes does not threaten the properties established in the frictionless case:

Theorem 3.2. *We consider a numerical flux function H consistent with the exact flux in the sense of (16), verifying the conservativity property (17). Assume that $(w_i^n)_{i\in\mathbb{Z}}$ belongs to Ω. We consider the updated states $(w_i^{n+1})_{i\in\mathbb{Z}}$ obtained with the scheme (29).*

1 *Under the CFL condition (19), supplemented by the following CFL restriction:*

$$
\Delta t \max_{i\in\mathbb{Z},\, j\in K_i} \Big[\frac{l_{ij}}{|T_{ij}|}\alpha_{ij}\Big(\max\big(0, H^h(W_i, W_j, \vec{n}_{ij})\big) - \min\big(0, \mathcal{H}^h(W_i).\vec{n}_{ij}\big)\Big] < \eta_i^n , \tag{34}
$$

we have $h_i^{n+1} \geq 0$, for all $i \in \mathbb{Z}$.

2 *Well balancing: assume $u_i^n = u_j^n = 0$ and $\eta_i^n = \eta_j^n = \eta$ for all $j \in K_i$. Then $u_i^{n+1} = 0$ and $\eta_i^{n+1} = \eta$.*

Proof. Concerning the motionless steady states preservation, starting from $W_i = W_j = {}^t(\eta, 0, 0)$, it can be readily appreciated that $\phi(w_i, w_i, \vec{n}_{ij}) = \phi(w_i, w_j, \vec{n}_{ij})$ and $\Delta F_{ij} = B_{ij} = 0$ for all $j \in K_i$, which gives $w_i^{n+1} = w_i^n$ in (29), that is the preservation of the static state.

Let's now focus on the robustness property. For the sake of simplicity, we will denote $H^h_{ij} := H^h(W_i, W_j, \vec{n}_{ij})$. According to the definition (13) and the consistency relation (16), we write:

$$\begin{aligned}\phi(w_i, w_j, \vec{n}_{ij}) &= \mathcal{X}_{ij} H^h_{ij} = \frac{1}{2}(\xi_i + \xi_j) H^h_{ij} - \frac{1}{2}(\xi_j - \xi_i)|H^h_{ij}| \\ &= \xi_i \,\frac{1}{2}(H^h_{ij} + |H^h_{ij}|) + \xi_j \,\frac{1}{2}(H^h_{ij} - |H^h_{ij}|)\,, \\ \phi(w_i, w_i, \vec{n}_{ij}) &= \mathcal{X}_{ii}\mathcal{H}^h(W_i).\vec{n}_{ij}\,.\end{aligned}$$

Thereafter, remembering that the current scheme is built on formulas (11), (23):

$$\begin{aligned}\tilde{h}^{n+1}_{ij} &= h^n_i - \frac{\Delta t}{\Delta_{ij}}\Big[\alpha_{ij}\phi^h(w_i, w_j, \vec{n}_{ij}) - \alpha^c_{ij}\phi^h(w_i, w_i, \vec{n}_{ij})\Big] + \frac{\Delta t}{\Delta_{ij}}(\alpha_{ij} - \alpha^c_{ij})\phi^h(w_i, w_i, \vec{n}_{ij}) \\ &= \xi_j \frac{\Delta t \alpha_{ij}}{2\Delta_{ij}}(|H^h_{ij}| - H^h_{ij}) + \Big[h^n_i - \xi_i \frac{\Delta t \alpha_{ij}}{2\Delta_{ij}}(H^h_{ij} + |H^h_{ij}|) + \frac{\Delta t \alpha_{ij}}{\Delta_{ij}}\mathcal{X}_{ii}\mathcal{H}^h(W_i).\vec{n}_{ij}\Big].\end{aligned}$$

The first term of this last expression being positive, we focus on the positivity of the second one, equivalent to the following condition, after factorization by $\xi_i = h_i/\eta_i \geq 0$:

$$\eta^n_i - \frac{\Delta t \alpha_{ij}}{\Delta_{ij}}\Big(\max(0, H^h(W_i, W_j, \vec{n}_{ij}) - \mathcal{H}^h(W_i).\vec{n}_{ij}\Big) \geq 0\,. \tag{35}$$

Under (34), we have (35). The proof is complete. □

4. Asymptotic preserving scheme

This section is devoted to the construction of an asymptotic preserving correction of the previous scheme. From a general point of view, most of theoretical and numerical studies have been developed in a 1D framework and marginal considerations have been given to the 2D case on unstructured triangulations. The novelty introduced in the following consists of constructing a numerical scheme which is able to restore the asymptotic diffusive regime satisfied by the late-time solutions of the 2D shallow water system. We highlight in Section 6 that working with asymptotic preserving schemes turns out to be essential to have a correct description of some flows, especially when dry areas are involved, in which case the asymptotic regime is immediately reached.

We aim at building a scheme for the discretization of the friction term that allows us to recover the expected asymptotic regime (9) satisfied by the solutions of system (1). To achieve this, we slightly modify the formulation of the source proposed in (21), writing:

$$\mathcal{F}(w) = \hat{\sigma}(\overline{R}(w) - w)\,, \tag{36}$$

where

$$\hat{\sigma} = \sigma + \overline{\sigma} \quad , \quad \overline{R}(w) = \left(\frac{\sigma}{\hat{\sigma}}R(w) + \frac{\overline{\sigma}}{\hat{\sigma}}w\right),$$

and σ, R are given by (22). The free parameter $\overline{\sigma}$ is introduced in order to reach the desired asymptotic preserving property, and will be set in the following. From now, the friction parameters in the scheme (23) are written as follows:

$$\alpha_{ij} = \frac{2\,\nu_i\, a_{ij}}{2\,\nu_i\, a_{ij} + \hat{\sigma}_{ij}\frac{|C_i|}{l_{ij}}}\,, \tag{37}$$

$$S^+_{ii} = a_{ii}\left(\overline{R}(w_i) - w_i\right) + \phi(w_i, w_i, \vec{n}_{ij})\,, \tag{38}$$

$$S^-_{ij} = -a_{ij}\left(w_i - \overline{R}(w_i)\right) - \phi(w_i, w_i, \vec{n}_{ij})\,. \tag{39}$$

Noting that we have $\overline{R}(w) - w = \begin{pmatrix} 0 \\ -\frac{\sigma}{\hat{\sigma}}\|\mathbf{q}\|\mathbf{q}\end{pmatrix}$, we obtain from (24) the following expression for the components of $\Delta S_{ij} = {}^t(\Delta S^h_{ij}, \Delta S^{\mathbf{q}}_{ij})$:

$$\begin{aligned}\Delta S^h_{ij} &= (\alpha_{ij} - \alpha^c_{ij})\phi^h(w_i, w_i, \vec{n}_{ij}), \\ \Delta S^{\mathbf{q}}_{ij} &= -\frac{\sigma_{ii}}{\hat{\sigma}_{ii}}(1 - \alpha^c_{ij}) a_{ii}\|\mathbf{q}_i\|\mathbf{q}_i - \frac{\sigma_{ij}}{\hat{\sigma}_{ij}}(1 - \alpha_{ij}) a_{ij}\|\mathbf{q}_i\|\mathbf{q}_i + (\alpha_{ij} - \alpha^c_{ij})\phi^{\mathbf{q}}(w_i, w_i, \vec{n}_{ij})\,,\end{aligned} \tag{40}$$

and reformulate the second equation using (37) as

$$\Delta S_{ij}^{\mathbf{q}} = -\frac{|C_i|}{l_{ij}}\left[\frac{a_{ii}\,\sigma_{ii}}{2\,\nu_i\,a_{ii}+\hat{\sigma}_{ii}|C_i|/l_{ij}} + \frac{a_{ij}\,\sigma_{ij}}{2\,\nu_i\,a_{ij}+\hat{\sigma}_{ij}|C_i|/l_{ij}}\right]\|\mathbf{q}_i\|\mathbf{q}_i + (\alpha_{ij}-\alpha_{ij}^{c})\phi^{\mathbf{q}}(w_i,w_i,\vec{n}_{ij})\,. \tag{41}$$

Considering the rescaling $\Delta t \longleftarrow \Delta t/\epsilon$, $\sigma_{ij} \longleftarrow \sigma_{ij}/\epsilon$, $\overline{\sigma}_{ij} \longleftarrow \overline{\sigma}_{ij}/\epsilon$ in (23), where ϵ is devoted to tend to zero, a brief study of the terms (41) gives $\mathbf{q}_i = 0$. Denoting α_{ij}^{ϵ} the corresponding rescaled friction parameter (37), we also have:

$$\frac{\Delta t}{\epsilon}\alpha_{ij}^{\epsilon} \underset{\epsilon\to 0}{\longrightarrow} \Delta t\frac{2\,\nu_i\,a_{ij}}{\hat{\sigma}_{ij}|C_i|/l_{ij}}\,.$$

Consequently, at the fully discrete level, the asymptotic behavior of the water height issuing from (23) reads:

$$\tilde{h}_{ij}^{n+1} = h_i^n - \frac{\Delta t}{\Delta_{ij}|C_i|/l_{ij}}\left[\frac{2\,\nu_i\,a_{ij}}{\hat{\sigma}_{ij}}\phi^h(w_i,w_j,\vec{n}_{ij}) - \frac{2\,\nu_i\,a_{ii}}{\hat{\sigma}_{ii}}\phi^h(w_i,w_i,\vec{n}_{ij})\right]_{|\mathbf{q}=0}. \tag{42}$$

We point out that this formula also holds for varying bathymetry profiles. Since the discharge vanishes as ϵ tends to zero (and so does the velocity), the choice of Rusanov fluxes yields:

$$\phi^h(w_i,w_j,\vec{n}_{ij})_{|\mathbf{u}=0} = \mathcal{X}_{ij}H^h(W_i,W_j,\vec{n}_{ij})_{|\mathbf{u}=0} = -\frac{a_{ij}}{2}\mathcal{X}_{ij}(\eta_j-\eta_i)\,,$$

$$\phi^h(w_i,w_i,\vec{n}_{ij})_{|\mathbf{u}=0} = 0\,,$$

and we obtain the following limit equation satisfied by the water height:

$$h_i^{n+1} = \sum_{j\in K_i}\frac{|T_{ij}|}{|C_i|}\tilde{h}_{ij}^{n+1}\,,$$

$$\tilde{h}_{ij}^{n+1} = h_i^n + \frac{\Delta t}{\Delta_{ij}|C_i|/l_{ij}}\frac{\mathcal{X}_{ij}\,\nu_i\,(a_{ij})^2}{\hat{\sigma}_{ij}}(\eta_j-\eta_i)\,,$$

that is:

$$h_i^{n+1} = h_i^n + \frac{\Delta t}{|C_i|}\sum_{j\in K_i}\frac{(l_{ij})^2}{|C_i|}\frac{\mathcal{X}_{ij}\,\nu_i\,(a_{ij})^2}{\hat{\sigma}_{ij}}(\eta_j-\eta_i)\,. \tag{43}$$

Now, we seek a relevant choice of $\hat{\sigma}_{ij}$ allowing to recover a given discretization of the limit equation (9). Let us assume that a consistent FV discretization of the targeted nonlinear diffusive regime is available:

$$h_i^{n+1} = h_i^n + \frac{\Delta t}{|C_i|}\sum_{j\in K_i}\int_{\Gamma_{ij}} F(h,\nabla\eta)\nabla\eta\cdot\vec{n}_{ij}\,, \tag{44}$$

where $F : (h,\nabla\eta) \longmapsto \dfrac{\sqrt{h}}{\varrho(h)\sqrt{\|\nabla\eta\|}}$, and that this discretization can be expressed under the following general formulation:

$$h_i^{n+1} = h_i^n + \frac{\Delta t}{|C_i|}\sum_{j\in K_i} l_{ij}F_{ij}\,(G_{ij}\cdot\vec{n}_{ij})(\eta_j-\eta_i), \tag{45}$$

where $(G_{ij}\cdot\vec{n}_{ij})(\eta_j-\eta_i)$ and F_{ij} are discrete approximations of $\nabla\eta_{|\Gamma_{ij}}$ and $F(h,\nabla\eta)_{|\Gamma_{ij}}$ respectively, with $(G_{ij}\cdot\vec{n}_{ij}) \geq 0$. Then, identifying (43) and (45) leads to the following expression for $\hat{\sigma}_{ij}$:

$$\hat{\sigma}_{ij} = \frac{l_{ij}\mathcal{X}_{ij}\nu_i\,(a_{ij})^2}{|C_i|\,F_{ij}\,(G_{ij}\cdot\vec{n}_{ij})}, \tag{46}$$

so that the limit scheme (43) for the water height coincides with the targeted FV discretization (45) for the limit diffusive regime (9).

Remark 4.1. Taking into account the modifications (37)–(39), the new friction scheme with the asymptotic preserving correction is still given by the general formulation (29). As a consequence, we can reproduce without any modifications the proof of Theorem 3.2, initially performed for the uncorrected scheme, and consequently show that both the motionless steady states preservation and the water height positivity preservation properties still hold.

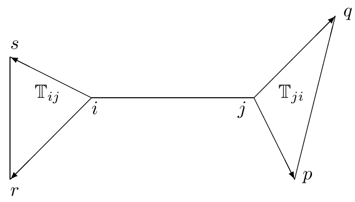

Fig. 5. Downstream and upstream triangles.

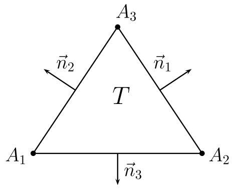

Fig. 6. $\mathbb{P}_1$ gradient approximation for a given element T.

5. Formal "second order" extension

In this section we propose to improve the accuracy of the scheme, following the reconstruction technique introduced in [24], and recently performed for the frictionless shallow water system (see [36]) based on the set of *pre-balanced* NSW equations. Actually, we aim at increasing the order of the current scheme evaluating in a better way the vector variable at each interface before the computation of the numerical fluxes. We choose to give a brief overview of this method, following closely the lines of [36]; considering $\mathbb{T}_{ij}$ and $\mathbb{T}_{ji}$ the downstream and upstream triangles related to two adjacent nodes i and j (see Fig. 5), we set:

$$\nabla \hat{w}_{ij}^{-} = \nabla \hat{w}_{\mathbb{T}_{ij}} \cdot \vec{ij} \quad , \quad \nabla \hat{w}_{ij}^{c} = \hat{w}_j - \hat{w}_i \quad , \quad \nabla \hat{w}_{ij}^{ho} = \frac{1}{3}\nabla \hat{w}_{ij}^{-} + \frac{2}{3}\nabla \hat{w}_{ij}^{c}\,, \tag{47}$$

where $\nabla \hat{w}_{T_k}$ denotes a $\mathbb{P}_1$ gradient approximation on the triangle T_k.

The present MUSCL reconstruction is performed on vertex-based geometries. As a consequence the $\mathbb{P}_1$ gradient approximation on a triangle can be directly determined having knowledge of the approximate solution at each of the three nodes. For a given element T, denoting $(A_i)_{i=1,\cdots,3}$ the nodes and $(\vec{n}_i)_{i=1,\cdots,3}$ the corresponding outward normals (see Fig. 6), the linear approximation of the variable on T reads:

$$w_T = \sum_{i=1}^{3} w_i l_i\,, \tag{48}$$

where $(l_i)_{i=1,\cdots,3}$ refers to the Lagrangian basis associated with T. More explicitly, one has, for a given point $M(x, y)$ in T:

$$l_i(M) = 1 - \frac{\overrightarrow{A_iM}.\vec{n}_i}{\|\overrightarrow{A_iA_j}\|}\,, \quad i = 1,2,3\,, \quad j \neq i\,, \tag{49}$$

so that we have:

$$\nabla w_T = -\sum_{i=1}^{3} w_i \frac{\vec{n}_i}{\|\overrightarrow{A_iA_j}\|}\,. \tag{50}$$

We consider now the three entries continuous limiter given by:

$$\mathcal{L}(a,b,c) = \begin{cases} 0 & \text{if} \quad \operatorname{sgn}(a) \neq \operatorname{sgn}(b), \\ \operatorname{sgn}(a)\min(|2a|, |2b|, |c|) & \text{otherwise}\,, \end{cases} \tag{51}$$

and write:

$$\mathcal{L}_{ij}(\hat{w}) = \mathcal{L}(\nabla \hat{w}_{ij}^{-}, \nabla \hat{w}_{ij}^{c}, \nabla \hat{w}_{ij}^{ho})\,. \tag{52}$$

At last, we can reach a better level of accuracy considering the following two values of the augmented vector variable $\hat{w} := (\eta, q_x, q_y, h)$ at each side of the interface Γ_{ij}:

$$\hat{w}_{ij} = \hat{w}_i + \frac{1}{2}\mathcal{L}_{ij}(\hat{w}) \quad , \quad \hat{w}_{ji} = \hat{w}_j - \frac{1}{2}\mathcal{L}_{ji}(\hat{w})\,. \tag{53}$$

Adopting the notations below:

$$\hat{w}_{ij} = {}^t(\eta_{ij}, (q_x)_{ij}, (q_y)_{ij}, h_{ij}) \quad , \quad \hat{w}_{ji} = {}^t(\eta_{ji}, (q_x)_{ji}, (q_y)_{ji}, h_{ji}), \tag{54}$$

the evaluation of the velocity and the fraction of water are performed as follows:

$$\mathbf{u}_{ij} = \mathbf{q}_{ij}/h_{ij} \quad , \quad \xi_{ij} = h_{ij}/\eta_{ij}, \tag{55}$$

so that the right flux at the edge Γ_{ij} becomes:

$$\phi(w_{ij}, w_{ji}, \vec{n}_{ij}) = \mathcal{X}_{ij} H(W_{ij}, W_{ji}, \vec{n}_{ij}), \tag{56}$$

with:

$$\begin{aligned} &W_{ij} = (\eta_{ij}, \eta_{ij}\mathbf{u}_{ij}) \quad , \quad W_{ji} = (\eta_{ji}, \eta_{ji}\mathbf{u}_{ji}), \\ &\mathcal{X}^*_{ij} = \begin{cases} \xi_{ij} & \text{if} \quad H^h(W_{ij}, W_{ji}, \vec{n}_{ij}) \geq 0, \\ \xi_{ji} & \text{otherwise}. \end{cases} \end{aligned} \tag{57}$$

We emphasize that we have $L_{ij}(\hat{w}) = 0$ whenever $w_i = w_j$. As a consequence, the left flux is still given by $\phi(w_i, w_i, \vec{n}_{ij}) = \mathcal{X}_{ii} H(W_i, W_i, \vec{n}_{ij})$. Finally, the high order scheme is also given by (29), substituting the right fluxes by those given by formula (56), and takes the form:

$$\begin{aligned} w_i^{n+1} = w_i^n - \frac{\Delta t}{|C_i|} \sum_{j \in K_i} l_{ij} \big[\alpha^*_{ij} \phi(w_{ij}, w_{ji}, \vec{n}_{ij}) - \alpha^*_{ij} \phi(w_i, w_i, \vec{n}_{ij})\big] \\ + \frac{\Delta t}{|C_i|} \sum_{j \in K_i} l_{ij} \Delta F^*_{ij} + \frac{\Delta t}{|C_i|} \sum_{j \in K_i} l_{ij} B^*_{ij}. \end{aligned} \tag{58}$$

Remark 5.1. Provided the use of "second order" transport relations for $\mathcal{X}^*_{ij}$ (57) and $\mathcal{N}^*_{ij}$ (similarly defined), the formulation of the components associated with the bed elevation (15) is also unchanged:

$$B^*_{ij} = \frac{g}{2} \begin{pmatrix} 0 \\ \mathcal{N}_{ii} \mathcal{N}^*_{ij} (\mathcal{X}^*_{ij} - \mathcal{X}_{ii}) \vec{n}_{ij} \end{pmatrix}. \tag{59}$$

As for the friction components α^*_{ij} and F^*_{ij}, their evaluation can equally be performed using the new values issuing from the reconstruction method. For the sake of simplicity we do not rewrite the explicit formula here, since the strategy simply consists of employing the reconstructed flow variable in (30) and (31).

Let us finally discuss the well balancing property of the MUSCL scheme:

Theorem 5.2. *We consider a numerical flux function H consistent with the exact flux in the sense of (16), verifying the conservativity property (17). Assume that $(w_i^n)_{i \in \mathbb{Z}}$ belongs to Ω. We consider the updated states $(w_i^{n+1})_{i \in \mathbb{Z}}$ obtained with the scheme (58). Assume $u_i^n = u_j^n = 0$ and $\eta_i^n = \eta_j^n = \eta$ for all $j \in K_i$. Then $u_i^{n+1} = 0$ and $\eta_i^{n+1} = \eta$.*

Proof. We notice that $\eta_{ij} = \eta_{ji} = \eta$ and $\mathbf{u}_{ij} = \mathbf{u}_{ji} = 0$ for $j \in K_i$. Hence, we have $\phi(w_{ij}, w_{ji}, \vec{n}_{ij}) = \mathcal{X}^*_{ij} g\eta^2/2 \begin{pmatrix} 0 \\ \vec{n}_{ij} \end{pmatrix}$, so that the contribution associated with the flux is given by:

$$\sum_{j \in K_i} l_{ij} \mathcal{X}^*_{ij} g\eta^2/2 \begin{pmatrix} 0 \\ \vec{n}_{ij} \end{pmatrix}. \tag{60}$$

We focus now on the contribution of the source. Highlighting that $\mathcal{N}^*_{ij} = \eta_{ij} = \eta$, we have $B^*_{ij} = g\eta^2/2 \begin{pmatrix} 0 \\ (\mathcal{X}^*_{ij} - \xi_i)\vec{n}_{ij} \end{pmatrix}$, and finally recover (60):

$$\sum_{j \in K_i} l_{ij} B^*_{ij} = \sum_{j \in K_i} l_{ij} \mathcal{X}^*_{ij} g\eta^2/2 \begin{pmatrix} 0 \\ \vec{n}_{ij} \end{pmatrix}, \tag{61}$$

according to Green's formula. $\square$

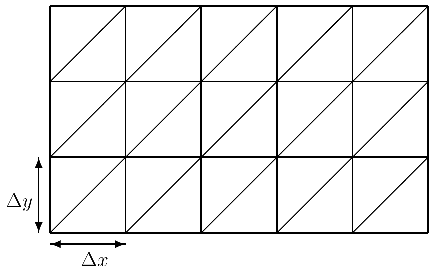

Fig. 7. Example of regular mesh.

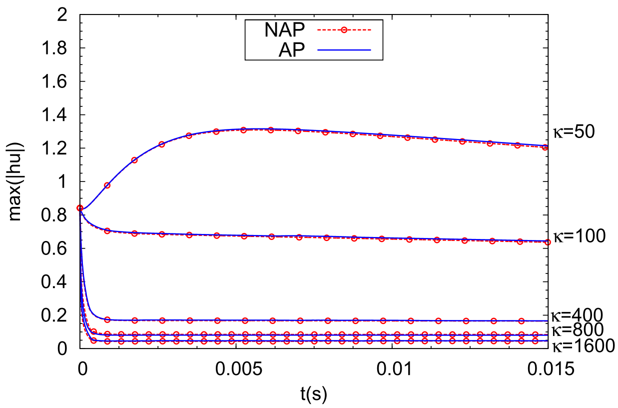

Fig. 8. Accuracy validation: Time series of the L^∞ norm of the discharge for increasing values of $\kappa = n^2$. AP scheme (*plain lines*) and NAP scheme (*circles*).

6. Numerical validations

In this section we present some numerical benchmark tests highlighting the relevance of this approach. We first pay attention to configurations involving dominant resistance effects, considering run-up on dry beds and/or high values of n for instance. As the scheme tends to reach its asymptotic limit behavior, we aim at highlighting the benefits of the asymptotic correction. We also point out the interest of considering low values of the water height; indeed, as it was specified in introductory lines, the treatment of low water height and/or dry cells areas may be source of instabilities. To highlight the efficiency of the high order scheme and perform convergence studies, we have to consider split Cartesian grids, which geometry is given by Fig. 7. Such meshes are also characterized by their horizontal and vertical discretization steps Δx and Δy, and will be called *regular* in the sequel. From a practical point of view, all the computations are performed using an explicit RK2 scheme for the time discretization. We distinguish corrected and uncorrected schemes calling them *AP scheme* and *NAP scheme* respectively. Finally, when nothing else is mentioned, the consideration of the resistance term will involve a Manning–Chezy formulation: the parameter γ in (3) is set to 10/3. Note that we use the classical form of Eqs. (1) and not the rescaled ones (5)–(7).

6.1. Accuracy validation

We perform this test to study the accuracy of the first and MUSCL schemes, as well as their behavior for increasing values of n. Initially, 1D and 2D versions have been proposed by Xing et al. [64]. This test case has also been adapted to evaluate the scheme developed in [11] for flows with friction, and we choose a 2D extrapolation. The channel dimensions are fixed to 1×0.2, and we use a regular mesh with $\Delta x = \Delta y = (1/60)$ m. Periodic boundary conditions are set both on left and right side regions. The topography is defined by the following function:

$$z(x, y) = \sin^2(\pi x),$$

and the initial flow vector is:

$$h(x, y, 0) = 5 + \exp(\cos(2\pi x)),$$

$$q_x(x, y, 0) = \sin(\cos(2\pi x)),$$

$$q_y(x, y, 0) = 0.$$

Time evolution of the L^∞ norm of the x-direction discharge for several values of $\kappa = n^2$ are shown in Fig. 8. We can note a very good agreement with the numerical predictions provided by the 1D scheme [11] for both AP and NAP scheme,

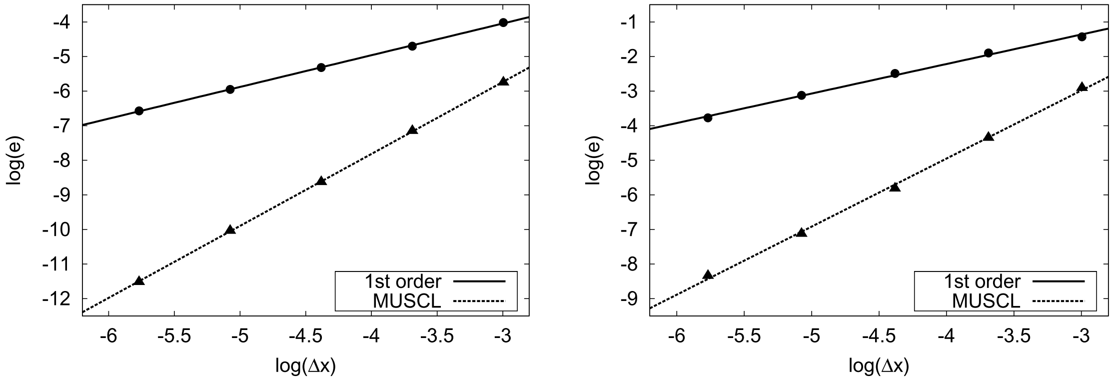

Fig. 9. Accuracy validation: L^1 error for h (*left*) and q_x (*right*) for increasing values of Δx (log–log scale).

even considering high values of n. The current friction approach exhibits good stability properties and, in particular, is able to account for varying bottoms whenever the friction terms are dominant.

As for the convergence rate analysis, several tests are performed with different values of the roughness coefficient. For a given n, a reference solution is computed with the MUSCL scheme on a 20 865 nodes regular mesh until $t = 0.1$ s, avoiding this way appearance of shocks, and then run simulations on a mesh series with increasingly refined triangulations: $\Delta x = \Delta y = 1/20, 1/40, 1/80, 1/160$ and $1/320$ m. Our numerical results are compared with the reference, which stands for an exact solution. Fig. 9 shows the evolution of the L^1 error on h and normal discharge q_x with respect to the mesh refinement for first and high order approaches in the case $n = 1$, in a log–log scale. As shown in Table 1, slopes of 0.9 and 2 are respectively reached up to $n = 10$, which is very satisfying for the description of a flow mainly controlled by friction effects, notably on unstructured grids (see [15,33]). Note that similar convergence rates can also be observed in [52] in the frictionless case. If the order of convergence is significantly improved by the MUSCL reconstruction up to $n = 50$ here, we observe that the benefits of the reconstruction is much attenuated when larger friction coefficients are used.

6.2. Oscillatory flows

The following two tests bring into play a periodic regime involving a planar flow with a non-zero resistance term, restraining the amplitude of the oscillations. We aim at validating the good behavior of the scheme near wet/dry interfaces and we study the accuracy of the shoreline location computation, for which an exact solution is available. For these tests, we use a linear friction source term:

$$\mathcal{F}(w) = \begin{pmatrix} 0 \\ k\mathbf{q} \end{pmatrix}.$$

Considering the low values of k involved in the simulations and the behavior of $\mathcal{F}$ as h tends to zero, the use of the asymptotic preserving correction is not justified here (and more generally for physical tests involving linear friction terms) and indeed, numerical investigations confirmed that the asymptotic correction was not useful here. Hence, we recover the formalism (21), setting this time $\sigma = k$ and $R(w) = {}^t(h, 0, 0)$, and run the computations with the original friction scheme of Section 3.

6.2.1. Moving boundary over a quadratic bottom

The first test is derived from a 1D experiment, usually encountered in the literature ([11,26] for example, or [11,9,49,53] for the parabolic version). Computations are performed on a 4320×500 regular grid with $\Delta x = 27$ m, $\Delta y = 25$ m, and the bed elevation is assumed to be defined as (see Fig. 10):

$$z(x, y) = h_0\big((x/a)^2 - 1\big).$$

The exact solution for the water depth elevation and the x-component of the velocity vector, obtained in [62], are given by:

$$\begin{cases} \eta(t,x,y) = \frac{a^2B^2e^{-kt}}{8g^2h_0}\Big(-sk\sin(2st) + (\frac{k^2}{4} - s^2)\cos(2st)\Big) - \frac{B^2e^{-kt}}{4g} - \frac{e^{-kt/2}}{g}\Big(Bs\cos(st) + \frac{kB}{2}\sin(st)\Big)x, \\ u(t) = Be^{-kt/2}\sin(st), \end{cases} \tag{62}$$

where $s = \sqrt{p^2 - k^2}$ and $p = \sqrt{8gh_0/a^2}$. The free surface is enforced at the left boundary, with $\eta(t, 0, y)$. As the moving water front is not supposed to reach the right side of the computational domain, no outflow boundary condition is imposed. The linear friction term is set to $k = 0.001$ and the other constants are $h_0 = 10$ m, $a = 3000$ m and $B = 2$ m/s. Considering the resistance effects in the exact solution, the flow is expected to converge toward a motionless steady state, while the

Table 1
Accuracy validation: convergence analysis – L^1 numerical error quantification and corresponding convergence rates for increasing Manning coefficients.

	Δx	1/20	1/40	1/80	1/160	1/320	Order
$n = 0$				**1st order**			
	h	1.9e−2	9.7e−3	5.3e−3	2.8e−3	1.5e−3	**0.9**
	q	2.6e−1	1.5e−1	8.8e−2	4.7e−2	2.4e−2	**0.9**
				MUSCL			
	h	3.5e−3	8.7e−4	1.9e−4	4.6e−5	1.0e−5	**2.1**
	q	5.9e−2	1.4e−2	3.2e−3	8.2e−4	2.3e−4	**2.0**
$n = 1$				**1st order**			
	h	1.9e−2	9.7e−3	5.3e−3	2.8e−3	1.5e−3	**0.9**
	q	2.6e−1	1.5e−1	8.8e−2	4.7e−2	2.4e−2	**0.9**
				MUSCL			
	h	3.5e−3	8.7e−4	1.9e−4	4.6e−5	1.0e−5	**2.1**
	q	5.9e−2	1.4e−2	3.2e−3	8.2e−4	2.3e−4	**2.0**
$n = 10$				**1st order**			
	h	1.8e−2	9.1e−3	4.9e−3	2.6e−3	1.4e−3	**0.9**
	q	2.4e−1	1.5e−1	8.3e−2	4.4e−2	2.3e−2	**0.8**
				MUSCL			
	h	3.2e−3	7.9e−4	1.8e−4	4.4e−5	1.0e−5	**2.1**
	q	5.5e−2	1.3e−2	3.0e−3	8.1e−4	2.4e−4	**2.0**
$n = 25$				**1st order**			
	h	1.3e−2	7.0e−3	3.6e−3	1.9e−3	9.8e−4	**0.9**
	q	2.1e−1	1.3e−1	6.8e−2	3.6e−2	1.9e−2	**0.9**
				MUSCL			
	h	1.9e−3	6.3e−4	1.9e−4	6.0e−5	1.7e−5	**1.7**
	q	4.1e−2	1.1e−2	3.9e−3	1.3e−3	3.6e−4	**1.7**
$n = 50$				**1st order**			
	h	7.9e−3	4.8e−3	2.4e−3	1.2e−3	6.5e−4	**0.9**
	q	1.6e−1	1.0e−1	5.5e−2	3.0e−2	1.6e−2	**0.8**
				MUSCL			
	h	1.4e−3	6.4e−4	2.7e−4	1.1e−4	3.7e−5	**1.3**
	q	3.7e−2	1.6e−2	7.4e−3	2.8e−3	8.9e−4	**1.4**
$n = 100$				**1st order**			
	h	6.7e−3	4.6e−3	2.8e−3	1.5e−3	8.3e−4	**0.8**
	q	1.2e−1	1.0e−1	5.5e−2	3.1e−2	1.7e−2	**0.8**
				MUSCL			
	h	2.1e−3	9.8e−4	5.3e−4	2.4e−4	8.3e−5	**1.2**
	q	1.0e−1	3.9e−2	1.8e−2	7.5e−3	2.5e−3	**1.3**

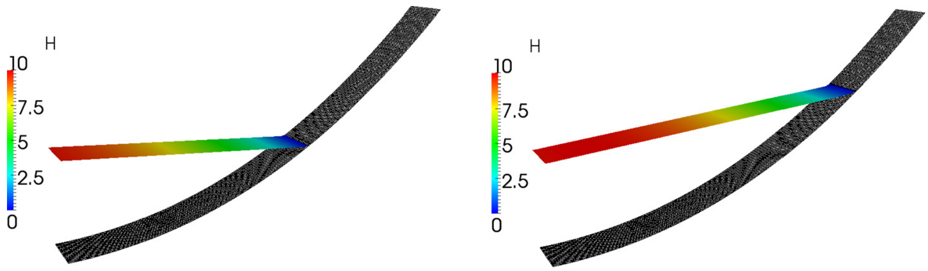

Fig. 10. Moving boundary over a quadratic bottom: mesh, topography and initial condition (left) and free surface level after a half period (right).

water free surface level will indefinitely oscillate in the frictionless case, with a half-period of 676.5 s. Impacts of the friction terms can be highlighted by Fig. 11, in which we follow the time evolution of the oscillating front until $t = 10\,000$ s. The predicted location of the wet/dry interface is very close to the theoretical one and we emphasize the good behavior of the proposed discretization, even for low values of h. Fig. 12 shows the total water depth surface at different times during a half period. Here again, we observe an excellent agreement between numerical and analytical results.

Accuracy analysis is performed using the analytical solution: estimations of L^1 error on the water height after a four period simulation are given in a logarithmic scale in Fig. 13 (left). Considering the impact on the convergence rate and the data available in Fig. 13 (right), we can point out the good performance of the formal second order scheme.

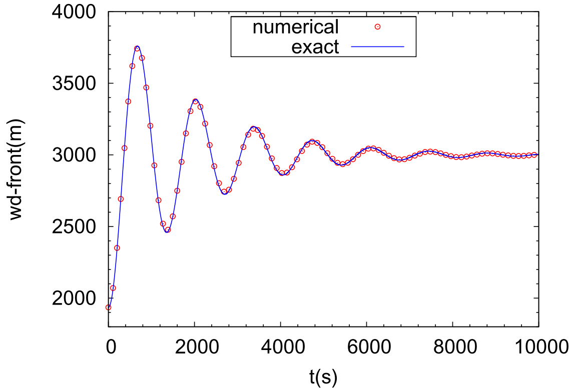

Fig. 11. Moving boundary over a quadratic bottom: time evolution of the wet/dry interface location.

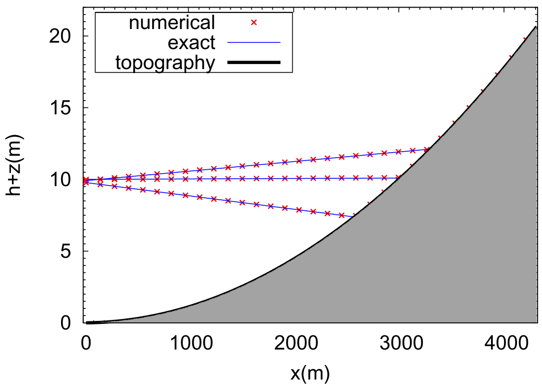

Fig. 12. Moving boundary over a quadratic bottom: free surface elevation along the x-direction centerline at times $t = 0$ s, 325 s and 650 s.

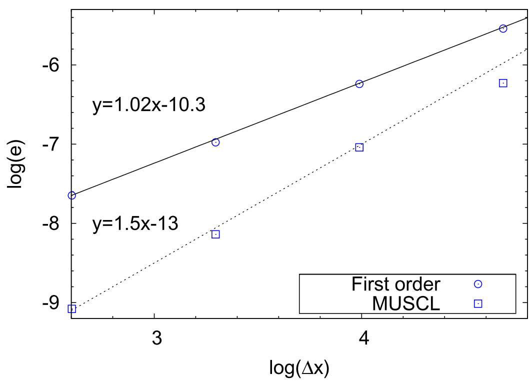

Δx	1st order	MUSCL
108	3.92e−3	1.97e−3
54	1.95e−3	8.76e−4
27	9.33e−4	2.92e−4
13.5	4.77e−4	1.14e−4

Fig. 13. Moving boundary over a quadratic bottom: L^1 error on h for first and high order schemes. Δx vs numerical error in a log–log scale, with corresponding slopes (left), and table of numerical errors (right).

6.2.2. Oscillatory flow in a parabolic bowl

In this test case, we want to assess the accuracy of our scheme in a real two dimensional framework, with an unstructured mesh, involving dry cells and varying topography. There are few available analytic solutions for frictional flows in the literature and the Thacker's 2D cases stand for discriminating benchmark tests. Two classes of exact solutions are available, namely the "*planar*" and "*curved*" cases, run for example in [15,36,40,50,58,61] and [15,38,61] respectively. Both are based on a parabolic topography of the form (see Fig. 14):

$$z(r) = r^2(h_0/a^2)\,, \tag{63}$$

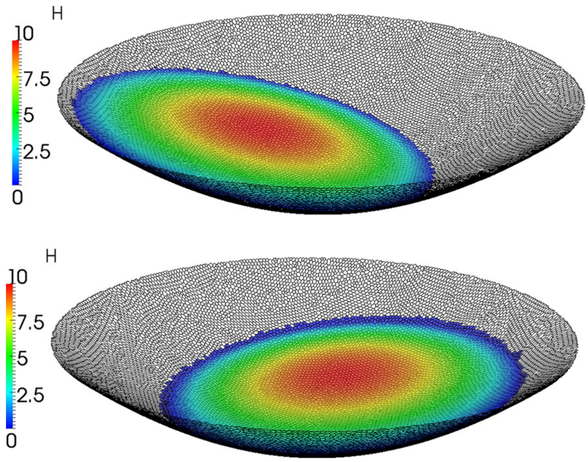

Fig. 14. Oscillatory flow with friction in a parabolic basin: mesh, geometry and initial condition (top) and free surface level after a half period (bottom).

where r is the distance from the center. We propose now to work on the 2D extrapolation of Thacker's parabolic test case introduced by Sampson et al. in [68] and also used in [63]. We consider here the planar free surface flow, with an exact motion given by:

$$\begin{cases} \eta(x,y,t) = h_0 - \dfrac{B^2}{2g}e^{-kt} - \dfrac{B}{g}e^{-kt/2}\Big(\dfrac{k}{2}\sin(st) + s\cos(st)\Big)x - \dfrac{B}{g}e^{-kt/2}\Big(\dfrac{k}{2}\cos(st) - s\sin(st)\Big)y\,, \\ u(t) = Be^{-kt/2}\sin(st)\,, \\ v(t) = -Be^{-kt/2}\cos(st)\,, \end{cases} \tag{64}$$

where $s = \sqrt{p^2 - k^2}/2$ and $p = \sqrt{8gh_0/a^2}$. In this test, the parameters are set to $h_0 = 10$ m, $a = 3000$ m, $B = 5$ m/s, and the linear friction coefficient is set to $k = 0.002$ s^{-1}. When friction effects are neglected, the exact solution describes an oscillatory flow with a half-period of 672 s. The initial condition is defined by evaluating (64) at $t = 0$. It provides a planar flow put in motion in the tangential direction. The corresponding profile is given in Fig. 14 (top), with an insight of the mesh and topography, together with a view of the flow after a half-period (bottom). We also recall that the theoretical shoreline location is given by:

$$x(t) = \frac{a^2}{2gh_0}e^{-kt/2}\Big(-B\,s\cos(s\,t) - \frac{1}{2}kB\sin(s\,t)\Big) \pm a\,. \tag{65}$$

We show in Fig. 15 some 2D views of the free surface along the middle section respectively after a half, one and two periods of evolution, supplemented by a comparison with the exact solution. We can observe an accurate description of the flow evolution. After four periods, the flow is almost at rest, as evidenced by the time history of wet/dry front location shown in Fig. 16. Again, in accordance with the theoretical solution, the free surface stays perfectly planar during the entire simulation time, notably in the neighborhood of dry areas. Numerical and theoretical values for the x- and y-velocity component at point $(1000, 0)$ are taken over a four period simulation and depicted in Fig. 17, allowing to follow the decay of the flow motion over time. Once again we can observe a reasonable correspondence between predicted and exact values. Note that similar results are obtained in [63], where the minor discrepancy on v can also be observed.

6.3. Dam break with friction

This test is devoted to highlight the impact of the asymptotic correction as the effects of the physical resistance become dominant. We proceed to a series of simulations of dam break problems in a rectangular channel $\Omega = [-10, 10] \times [-2, 2]$, on a flat bottom. The computational domain is initially meshed with a regular triangulation of 5884 nodes. The dam is supposed to be located at $x = 0$ along the y direction. The initial condition is:

$$h(x) = \begin{cases} h_g & \text{if} \quad x < 0\,, \\ h_d & \text{otherwise}, \end{cases} \qquad \text{with} \qquad h_g > h_d\,. \tag{66}$$

The first test consists of a non-physical case: we deliberately choose an excessive friction parameter n, and study the results given by the AP and NAP schemes. As the AP scheme is precisely designed to degenerate toward the discrete version of the asymptotic regime (9), the corresponding approximations should get closer as the time and the friction parameter increase. We set $n = 25$, $h_g = 2$ m, $h_d = 1$ m, and study the evolution of the flow until $t = 9$ s. Fig. 18 shows a middle section of the water height for both corrected and uncorrected schemes at the end of the simulation, put in comparison with the scheme

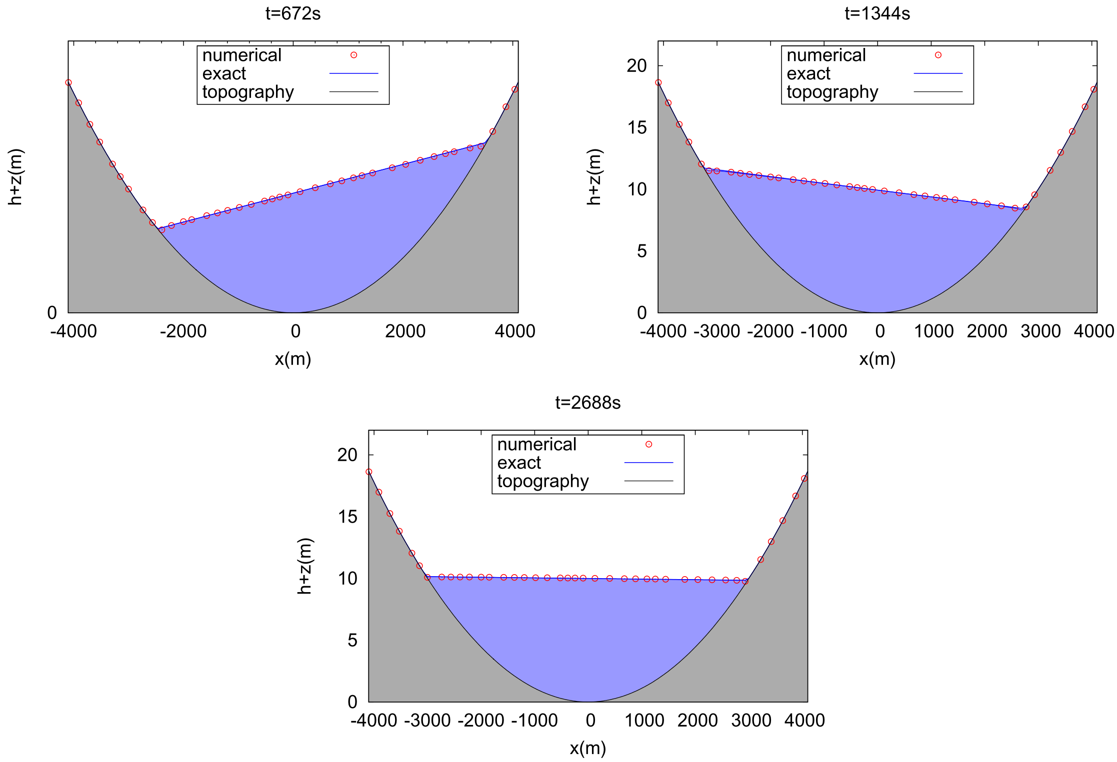

Fig. 15. Oscillatory flow with friction in a parabolic basin: free surface profiles at several times during the revolution process, and comparison with the analytic solution.

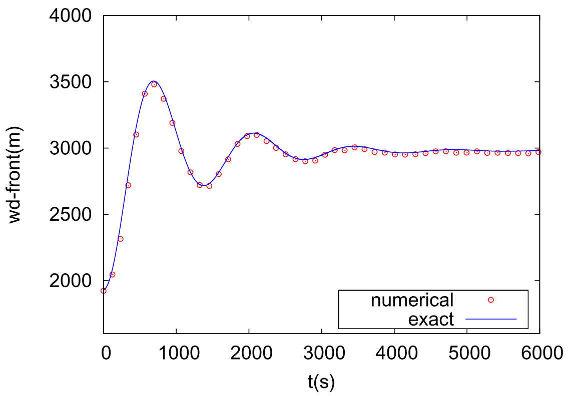

Fig. 16. Oscillatory flow with friction in a parabolic basin: shoreline location – analytic vs numeric.

used for the diffusive limit. We can clearly observe the impact of the modification on the limit behavior. Taking the limit regime as a reference, L^1 and L^∞ errors are quantified and plotted in Fig. 19. The trends emerging from this complementary error study confirm the relevance of the AP correction.

Let us now consider moderate values of the friction parameter, to identify the AP scheme's influence. First, we enforce the same left and right initial values for the water elevation, with this time $n = 0.1$. Considering the downstream water depth involved in this test, the asymptotic regime is far from being reached during the simulation, and the effects of the asymptotic correction are expected to be insignificant. Sections of the water surface profile along the x-direction are available in Fig. 20 at several times of the simulation. And indeed, AP and NAP schemes provide very close results. The curves are almost indistinguishable at this level of zoom. These observations tend to confirm the worthlessness of the correction when the water height levels involved in the simulation are relatively high, or when the friction term is not particularly stiff.

Before observing the impact in a dry bed context, we suggest an intermediate test, keeping $h_g = 2$ m and $n = 0.1$, and enforcing $h_d = 0.1$ m. As previously, we follow the evolution of the predicted flood wave elevation given by the two schemes. Results are plotted in Fig. 21, with a particular focus on the water front, highlighting some discrepancies. We reach

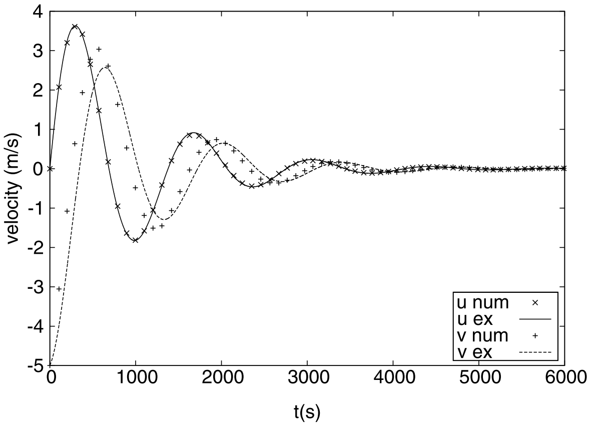

Fig. 17. Oscillatory flow with friction in a parabolic basin: time evolution of the x and y-direction velocity – analytic vs numeric.

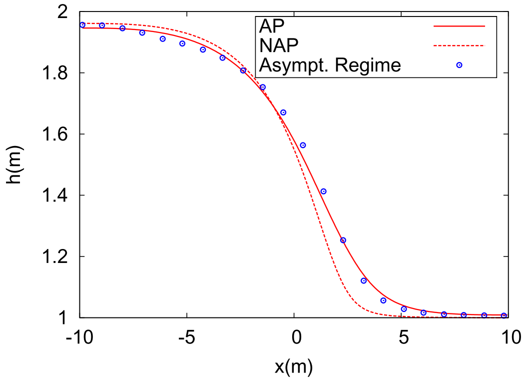

Fig. 18. Dam break with friction – test 1: $n = 25$, $h_g = 2$ m, $h_d = 1$ m. Middle section of the water depth profiles at $t = 9$ s – comparison with the asymptotic regime.

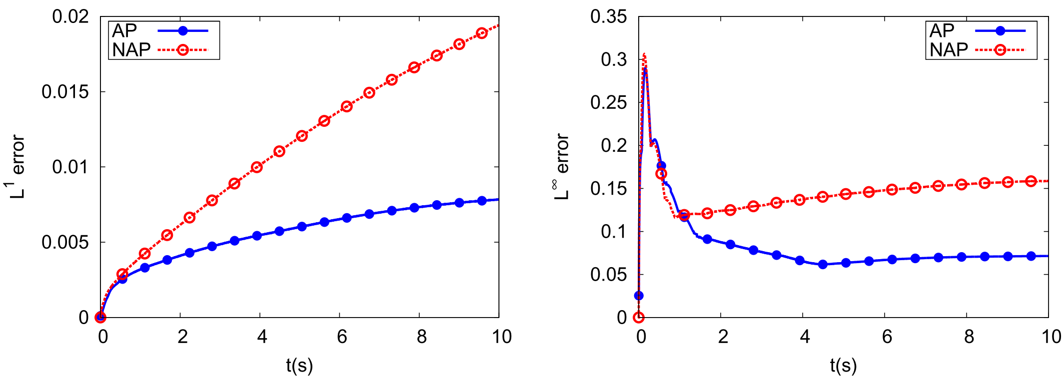

Fig. 19. Dam break with friction – test 1: L^1 (*left*) and L^∞ (*right*) error evolution.

a difference of 15 cm between the two predicted fronts at time $t = 2$ s. This time, considering the low value of h_d, both schemes get closer to their asymptotic behavior in the vicinity of the front location: the use of an asymptotic preserving scheme seems to be necessary to have a better evaluation of the flood wave velocity.

For the last configuration, we set $h_d = 0$ m. In this dry context, the asymptotic regime is immediately reached in the right side of the domain. We observe similar results than those provided by test 3 (Fig. 22), with a stronger impact of the correction: the location of the two fronts differs this time from almost $Dx = 30$ cm at the end of the simulation.

We finally study the behavior of the AP and NAP schemes for different values of h_g : 1, 2, 3, 4 and 5 m. We also improve the quality of the mesh, working with a 20 890 nodes regular triangulation. In Fig. 23 we can follow the evolution of the wet/dry interface location (left) for both AP and NAP schemes, supplemented by a visualization of the resulting gap Dx with respect to time (right) until $t = 2$ s. Numerical results clearly show that the impact of the correction is all the more

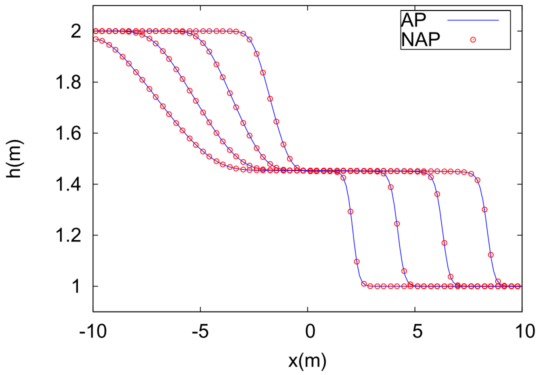

Fig. 20. Dam break with friction – test 2: $n = 0.1$, $h_g = 2$ m, $h_d = 1$ m. Middle section of the water depth profiles for both AP and NAP schemes at times $t = 0.5$, 1, 1.5 and 2 s.

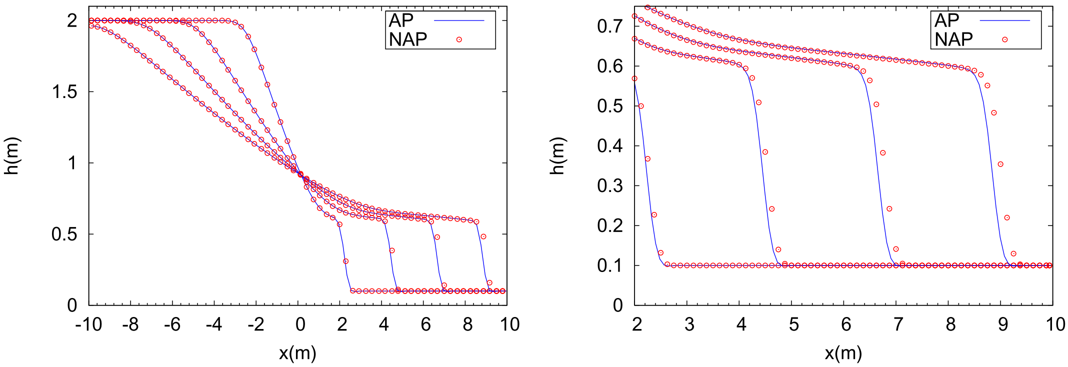

Fig. 21. Dam break with friction – test 3: $n = 0.1$, $h_g = 2$ m, $h_d = 0.1$ m. Middle section of the water depth profiles for AP and NAP schemes at times $t = 0.5$, 1, 1.5 and 2 s. General profile (left), and zoom on the water front (right).

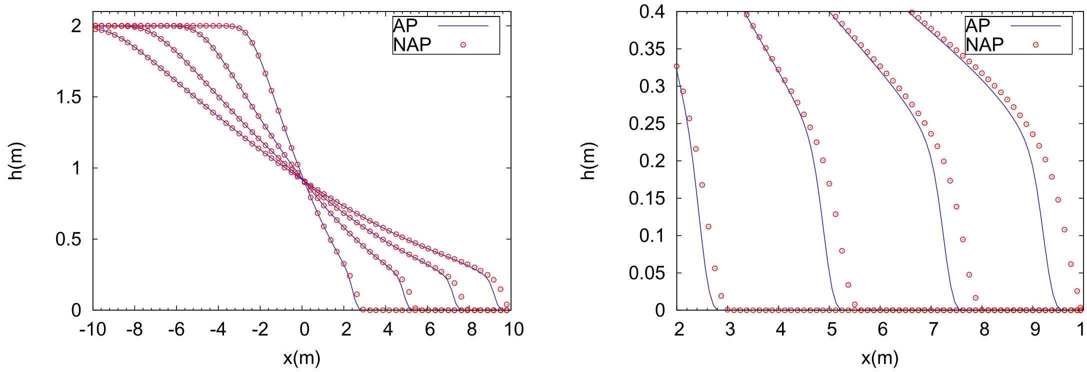

Fig. 22. Dam break with friction - test 4: $n = 0.1$, $h_g = 2$ m, $h_d = 0$ m. Middle section of the water depth profiles for AP and NAP schemes at times $t = 0.5$, 1, 1.5 and 2 s. General profile (left), and zoom on the water front (right).

pronounced since the initial jump is important. We also emphasize that the amplitude of the gap Dx does not decrease as the mesh is refined: the loss of accuracy related to the non-consideration of the limit regime restoration can definitively not be offset by an increase of the number of nodes. The use of an asymptotic preserving scheme seems to describe slightly different behaviors when compared to traditional approaches in such a context.

6.4. Dam-break flow over two frictional humps

We go ahead in the exploration of the friction scheme's abilities considering the 1D dam break experiment presented in [4]. The basin is 7 m length and its width is set to 1 m for purpose of a 2D application. Details on the topography are given in Fig. 24. In the physical model the base of the reservoir is located in the middle of the first plane area, that is $x = 2.25$ m, and the initial upstream free surface is set to 0.5 m. A Manning roughness coefficient $n = 0.01$ is imposed. Computations

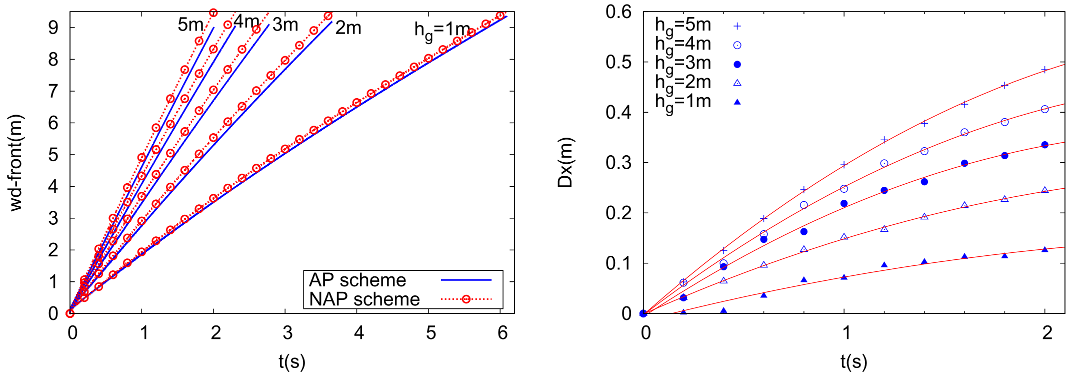

Fig. 23. Dam break with friction – test 5: location of the shoreline for the AP and NAP schemes (*left*) and flood wave gap Dx (*right*) for increasing values of h_g.

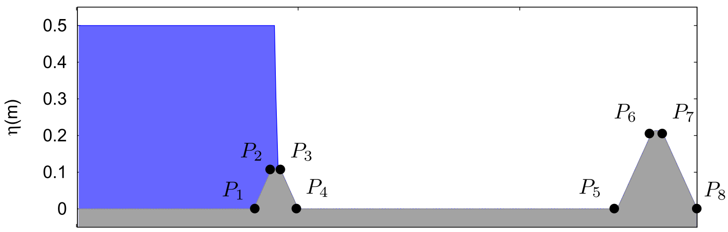

	x (m)	z (m)
P_1	2.00	0.000
P_2	2.20	0.108
P_3	2.30	0.108
P_4	2.50	0.000
P_5	6.10	0.000
P_6	6.50	0.213
P_7	6.60	0.213
P_8	7.00	0.000

Fig. 24. Dam-break flow over two frictional humps: sketch of the basin and initial condition.

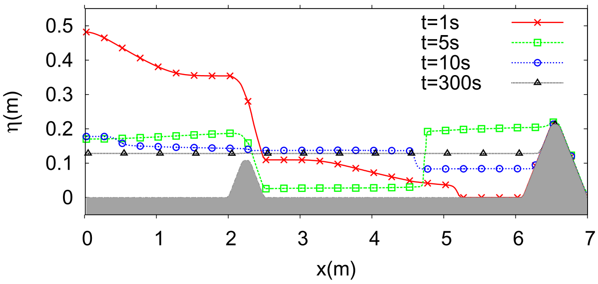

Fig. 25. Dam-break flow over two frictional humps: free surface profiles at $t = 1$, 5, 10 and 300 s.

are run on a regular triangulation made of 5901 vertices, corresponding to a space step $\Delta x = \Delta y = 0.025$ m. Reflective conditions are set at the lateral and upstream boundaries, and free outflow is assumed downstream. This test is particularly interesting to evaluate our scheme's ability, due to the complex topography variations, generating some flow reflections in the presence of a dry bed. We show in Fig. 25 a comparison between the computed free surface and the data, during the first steps of the propagation. We obtain very satisfying results, with an accurate computation of the wet/dry interface. Approximatively around $t = 300$ s, a motionless steady state is reached within the left portion of the domain. Very similar results are obtained in [50] with RKDG schemes. We finally plot in Fig. 26 the evolution of the water height up to $t = 15$ s computed at three reference points along the basin with both the AP and the NAP schemes, and compare our results with experimental data. We highlight that as friction effects dominate the flow in very shallow areas, the use of the AP scheme noticeably helps to obtain a satisfying matching with the data.

6.5. Malpasset dam break

The Malpasset dam break is one of the main dam-break benchmark tests for which experimental measurements are available. It relies on a 2D bathymetry involving a complex geometry (see Fig. 27). The foundations of this dam were based is the bed of the Reyran river valley, in the south of France. In December 1959, the left side of the dam collapsed under the effects of pressure, after a heavy rain fall; more than 55 000 m^3 of water started to pour in this narrow gorge, and the generated flood wave reached the city of Frejus, located 12 km downstream, making 433 casualties. For this test, the domain is meshed with 13 541 nodes. Maximum free surface elevation and propagation time of the water front are available at several points of the bed river; predicted arrival time of the flood wave at gauges 6 to 14 are plotted in Fig. 28, where n is fixed to 0.02; we can note a good agreement with the reference, and significant agreements with other published results

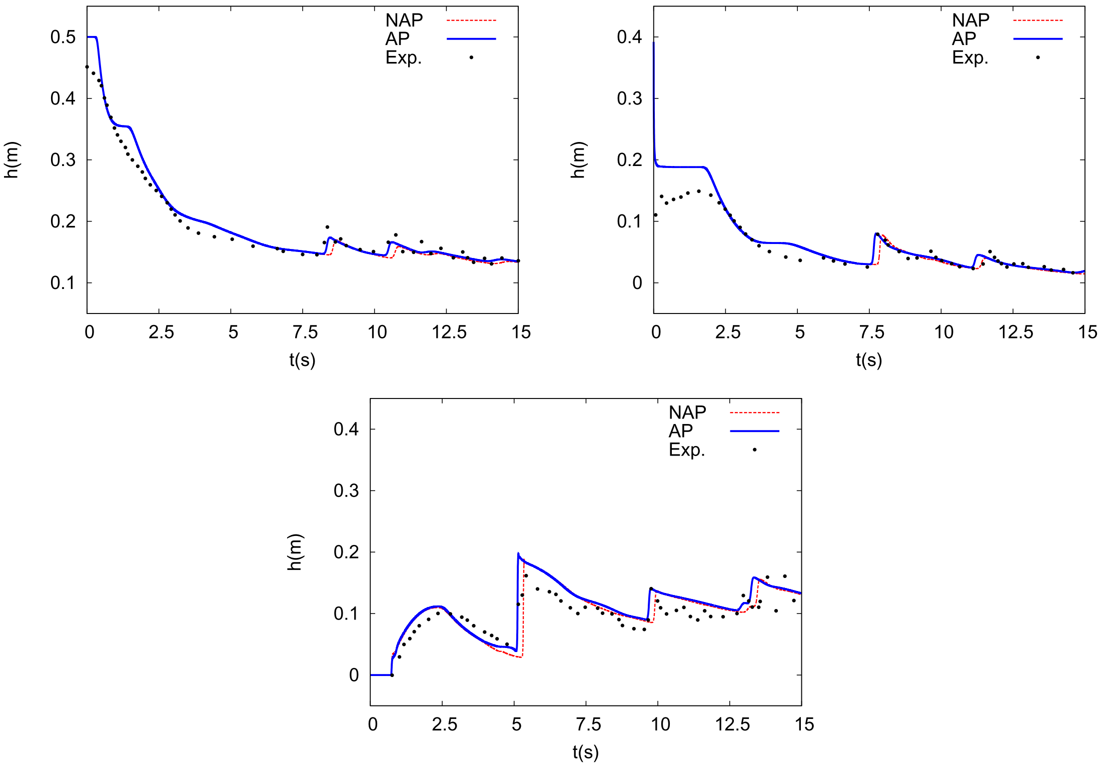

Fig. 26. Dam-break flow over two frictional humps: time history of the free surface and comparison between AP and NAP schemes.

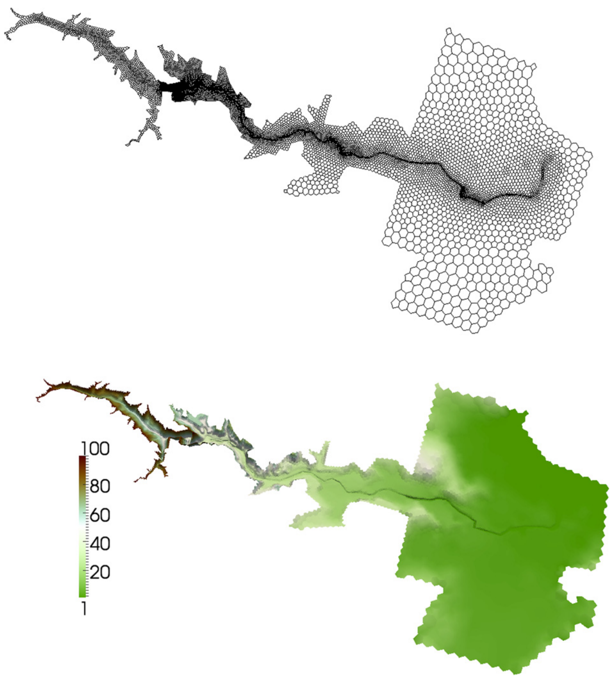

Fig. 27. Malpasset dam break: dual mesh geometry (top) and topography (bottom).

[20,63]. The use of friction source terms is unavoidable to obtain satisfying results. Comparisons with the AP scheme let appear discrepancies in the order of 2% with the measured values. As previously, carrying out the correction tends to slow down the evolution of the wave front in the floodplain.

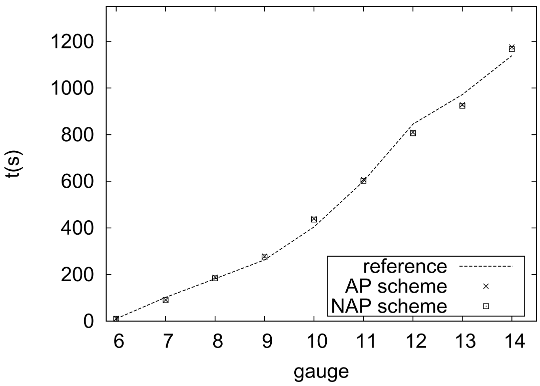

Gauge	Ref.	AP	NAP
6	10	11	10
7	102	91	90
8	182	188	184
9	263	279	274
10	404	440	436
11	600	608	602
12	845	810	806
13	972	928	924
14	1139	1176	1167

Fig. 28. Malpasset dam break: arrival time of the flood wave front at gauges 6 to 14.

7. Conclusion

In this work, we introduce a new way to account for the friction effects in the context of the 2D shallow water equations, extending the mono-dimensional approach proposed in [11] and [9]. The resulting scheme is shown to be well balanced and robust under some appropriate time step constraints. A formal second order reconstruction is also proposed. In addition, an asymptotic preserving correction is performed, which stands for a novelty in the context of unstructured triangulations. Numerical results clearly highlight the capabilities of the AP scheme in handling dry areas, in a large variety of test cases involving complex topography and geometry.

References

[1] D. Aregba-Driollet, M. Briani, R. Natalini, Asymptotic high order preserving schemes for 2 × 2 dissipative hyperbolic systems, SIAM J. Numer. Anal. 46 (2008) 869–894.
[2] E. Audusse, F. Bouchut, M.O. Bristeau, R. Klein, B. Perthame, A fast and stable well-balanced scheme with hydrostatic reconstruction for shallow water flows, SIAM J. Sci. Comput. 25 (2004) 2050–2065.
[3] E. Audusse, M.O. Bristeau, A well balanced positivity preserving “second-order” scheme for shallow water flows on unstructured meshes, J. Comput. Phys. 206 (2005) 311–333.
[4] F. Aureli, P. Mignosa, M. Tomirotti, Dam-break flows in presence of abrupt bottom variations, in: Proc. XXVIII IAHR Congr., Graz, Austria, 1999, pp. 163–171.
[5] F. Benkhaldoun, I. Elmahi, M. Seaid, A new finite volume method for flux-gradient and source-term balancing in shallow water equations, Comput. Methods Appl. Mech. Eng. 199 (2010) 3324–3335.
[6] A. Bermudez, M.-E. Vazquez, Upwind methods for hyperbolic conservation laws with source terms, Comput. Fluids 23 (1994) 1049–1071.
[7] C. Berthon, P. Charrier, B. Dubroca, An HLLC scheme to solve the M1 model of radiative transfer in two space dimensions, J. Sci. Comput. 31 (2007) 347–389.
[8] C. Berthon, J. Dubois, B. Dubroca, T.-H. Nguyen-Bui, R. Turpault, A free streaming contact preserving scheme for the M1 model, Adv. Appl. Math. Mech. 2 (2010) 259–285.
[9] C. Berthon, F. Foucher, Efficient well balanced hydrostatic upwind schemes for shallow water equations, J. Comput. Phys. 231 (2012) 4993–5015.
[10] C. Berthon, P. LeFloch, R. Turpault, Late-time/stiff-relaxation asymptotic-preserving approximations of hyperbolic equations, Math. Comput. 82 (2013) 831–860.
[11] C. Berthon, F. Marche, R. Turpault, An efficient scheme on wet/dry transitions for shallow water equations with friction, Comput. Fluids 48 (2011) 192–201.
[12] C. Berthon, R. Turpault, Asymptotic preserving HLL schemes, Numer. Methods Partial Differ. Equ. 27 (2011) 1396–1422.
[13] S. Bianchini, B. Hanouzet, R. Natalini, Asymptotic behavior of smooth solutions for partially dissipative hyperbolic systems with a convex entropy, Commun. Pure Appl. Math. 60 (2007) 1559–1622.
[14] O. Bokhove, Flooding and drying in finite-element discretizations of shallow-water equations. Part 2: two dimensions, 2003. Imported from MEMORANDA.
[15] A. Bollermann, S. Noelle, M. Lukacova-Medvidova, Finite volume evolution Galerkin methods for the shallow water equations with dry beds, Commun. Comput. Phys. 10 (2011) 371–404.
[16] F. Bouchut, Nonlinear Stability of Finite Volume Methods for Hyperbolic Conservation Laws, and Well-Balanced Schemes for Sources, Frontiers in Mathematics, Birkhäuser, 2004.
[17] F. Bouchut, H. Ounaissa, B. Perthame, Upwinding of the source term at interfaces for Euler equations with high friction, Comput. Math. Appl. 53 (2007) 361–375.
[18] S.F. Bradford, B.F. Sanders, Finite-volume model for shallow-water flooding of arbitrary topography, J. Hydrol. Eng. 128 (2002) 289–298.
[19] M.-O. Bristeau, B. Coussin, Boundary conditions for the shallow water equations solved by kinetic schemes, INRIA Report RR-4282, 2001, http://www.inria.fr/RRRT/RR-4282.html.
[20] A.R. Brodtkorb, M.L. Sætra, M. Altinakar, Efficient shallow water simulations on GPUs: implementation, visualization, verification and validation, Comput. Fluids 55 (2012) 1–12.
[21] C. Buet, S. Cordier, An asymptotic preserving scheme for hydrodynamics radiative transfer models: numerical scheme for radiative transfer, Numer. Math. 108 (2007) 199–221.
[22] C. Buet, B. Després, Asymptotic preserving and positive schemes for radiation hydrodynamics, J. Comput. Phys. 215 (2006) 717–740.
[23] C. Buet, B. Després, E. Franck, Design of asymptotic preserving finite volume schemes for the hyperbolic heat equation on unstructured meshes, Numer. Math. 122 (2012) 227–278.

[24] S. Camarri, M.V. Salvetti, B. Koobus, A. Dervieux, A low-diffusion muscl scheme for LES on unstructured grids, Comput. Fluids 33 (2004) 1101–1129.
[25] M. Castro, A. Milanes, C. Pares, Well-balanced numerical schemes based on a generalized hydrostatic reconstruction technique, Math. Models Methods Appl. Sci. 17 (2007) 2055–2113.
[26] L. Cea, M.E. Vázquez-Cendón, Unstructured finite volume discretization of bed friction and convective flux in solute transport models linked to the shallow water equations, J. Comput. Phys. 231 (2012) 3317–3339.
[27] C. Cercignani, The Boltzmann Equation and Its Applications, Appl. Math. Sci., vol. 67, Springer-Verlag, New York, 1988.
[28] C. Chalons, F. Coquel, E. Godlewski, P.-A. Raviart, N. Seguin, Godunov-type schemes for hyperbolic systems with parameter dependent source. The case of Euler system with friction, Math. Models Methods Appl. Sci. 20 (2010) 2109–2166.
[29] G.Q. Chen, C.D. Levermore, T.P. Liu, Hyperbolic conservation laws with stiff-relaxation terms and entropy, Commun. Pure Appl. Math. 47 (1995) 787–830.
[30] F. Coquel, B. Perthame, Relaxation of energy and approximate Riemann solvers for general pressure laws in fluid dynamics, SIAM J. Numer. Anal. 35 (1998) 2223–2249.
[31] P. Crispel, P. Degond, M.-H. Vignal, An asymptotic preserving scheme for the two-fluid Euler–Poisson model in the quasi-neutral limit, J. Comput. Phys. 223 (2007) 208–234.
[32] P. Degond, F. Deluzet, A. Sangam, M.-H. Vignal, A numerical scheme for a viscous shallow water model with friction, J. Comput. Phys. 228 (2009) 3540–3558.
[33] O. Delestre, F. Marche, A numerical scheme for a viscous shallow water model with friction, J. Sci. Comput. 48 (2011) 41–51.
[34] A.I. Delis, N.A. Kampanis, Numerical flood simulation by depth averaged free surface flow models, in: Environmental Systems – Encyclopedia of Life Support Systems (EOLSS), 2009.
[35] B. Dubroca, J.-L. Feugeas, Entropic moment closure hierarchy for the radiative transfer equation, C. R. Acad. Sci. Paris 329 (1999) 915–920.
[36] A. Duran, F. Marche, Q. Liang, On the well-balanced numerical discretization of shallow water equations on unstructured meshes, J. Comput. Phys. 235 (2013) 565–586.
[37] D. Dutykh, R. Poncet, F. Dias, The VOLNA code for the numerical modelling of tsunami waves: generation, propagation and inundation, Eur. J. Mech. B, Fluids 30 (2011) 598–615.
[38] A. Ern, S. Piperno, K. Djadel, A well-balanced Runge–Kutta discontinuous Galerkin method for the shallow-water equations with flooding and drying, Int. J. Numer. Methods Fluids 58 (2008) 1–25.
[39] E. Franck, Construction et analyse numérique de schémas “asymptotic preserving” sur maillages non structurés. Application à l'équation de transport et aux systèmes de Friedrichs, PhD thesis, 2012.
[40] J.M. Gallardo, C. Parés, M. Castro, On a well-balanced high-order finite volume scheme for shallow water equations with topography and dry areas, J. Comput. Phys. 227 (2007) 574–601.
[41] L. Gosse, G. Toscani, An asymptotic-preserving well-balanced scheme for the hyperbolic heat equations, C. R. Acad. Sci. Paris 334 (2002) 337–342.
[42] L. Gosse, G. Toscani, Space localization and well-balanced schemes for discrete kinetic models in diffusive regimes, SIAM J. Numer. Anal. 41 (2003) 641–658.
[43] J.M. Greenberg, A.Y. Leroux, A well-balanced scheme for the numerical processing of source terms in hyperbolic equations, SIAM J. Numer. Anal. 33 (1996) 1–16.
[44] S. Jin, Efficient asymptotic-preserving (AP) schemes for some multiscale kinetic equations, SIAM J. Sci. Comput. 21 (1999) 441–454.
[45] S. Jin, A steady-state capturing method for hyperbolic systems with geometrical source terms, Modél. Math. Anal. Numér. 35 (2001) 631–645.
[46] S. Jin, D. Levermore, Numerical schemes for hyperbolic conservation laws with stiff relaxation terms, J. Comput. Phys. 126 (1996) 449–467.
[47] T. Katsaounis, B. Perthame, C. Simeoni, Upwinding sources at interfaces in conservation laws, Appl. Math. Lett. 17 (2004) 309–316.
[48] G. Kesserwani, Q. Liang, A discontinuous Galerkin algorithm for the two-dimensional shallow water equations, Comput. Methods Appl. Mech. Eng. 199 (2010) 3356–3368.
[49] G. Kesserwani, Q. Liang, Well-balanced RKDG2 solutions to the shallow water equations over irregular domains with wetting and drying, Comput. Fluids 39 (2010) 2040–2050.
[50] G. Kesserwani, Q. Liang, Locally limited and fully conserved RKDG2 shallow water solutions with wetting and drying, J. Sci. Comput. 50 (2012) 120–144.
[51] A. Kurganov, D. Levy, Central-upwind schemes for the Saint-Venant system, Math. Model. Numer. Anal. 36 (2002) 397–425.
[52] A. Kurganov, G. Petrova, A second-order well-balanced positivity preserving central-upwind scheme for the Saint-Venant system, Commun. Math. Sci. 5 (2007) 133–160.
[53] Q. Liang, F. Marche, Numerical resolution of well-balanced shallow water equations with complex source terms, Adv. Water Resour. 32 (2009) 873–884.
[54] P.L. Lions, G. Toscani, Diffusive limit for finite velocity Boltzmann kinetic models, Rev. Mat. Iberoam. 13 (1997) 473–513.
[55] M. Lukacova-Medvidova, S. Noelle, M. Kraft, Well-balanced finite volume evolution Galerkin methods for the shallow water equations, J. Comput. Phys. 1 (2007) 122–147.
[56] P. Marcati, A. Milani, The one-dimensional Darcy's law as the limit of a compressible Euler flow, J. Differ. Equ. 84 (1990) 129–146.
[57] F. Marche, P. Bonneton, P. Fabrie, N. Seguin, Evaluation of well-balanced bore-capturing schemes for 2D wetting and drying processes, Int. J. Numer. Methods Fluids 53 (2007) 867–894.
[58] I.K. Nikolos, A.I. Delis, An unstructured node-centered finite volume scheme for shallow water flows with wet/dry fronts over complex topography, Comput. Methods Appl. Mech. Eng. 198 (2009) 3723–3750.
[59] S. Noelle, N. Pankratz, G. Puppo, J.R. Natvig, Well-balanced finite volume schemes of arbitrary order of accuracy for shallow water flows, J. Comput. Phys. 213 (2006) 474–499.
[60] B. Perthame, C. Simeoni, A kinetic scheme for the Saint-Venant system with a source term, Calcolo 38 (2001) 201–231.
[61] M. Ricchiuto, A. Bollermann, Stabilized residual distribution for shallow water simulations, J. Comput. Phys. 228 (2009) 1071–1115.
[62] J. Sampson, A. Easton, M. Singh, Moving boundary shallow water flow above parabolic bottom topography, in: EMAC 2005, ANZIAM J. 21 (2006) 373–387.
[63] Y. Wang, Q. Liang, G. Kesserwani, J.W. Hall, A 2D shallow flow model for practical dam-break simulations, J. Hydraul. Res. 49 (2011) 307–316.
[64] Y. Xing, C.-W. Shu, High order finite difference WENO schemes with the exact conservation property for the shallow water equations, J. Comput. Phys. 208 (2005) 206–227.
[65] Y. Xing, C.-W. Shu, A new approach of high order well-balanced finite volume WENO schemes and discontinuous Galerkin methods for a class of hyperbolic systems with source terms, Commun. Comput. Phys. 1 (2006) 100–134.
[66] Y. Xing, X. Zhang, Positivity-preserving well-balanced discontinuous Galerkin methods for the shallow water equations on unstructured triangular meshes, J. Sci. Comput. 57 (2013) 19–41.
[67] J.G. Zhou, D.M. Causon, C.G. Mingham, The surface gradient method for the treatment of source terms in the shallow-water equations, J. Comput. Phys. 168 (2001) 1–25.
[68] J. Sampson, A. Easton, M. Singh, Moving boundary shallow water flow in circular paraboloidal basins, in: Proceedings of the Sixth Engineering Mathematics and Applications Conference, 5th International Congress on Industrial and Applied Mathematics, 2003, pp. 223–227.